

Ash plume top height estimate using AATSR

T. H. Virtanen et al.

This discussion paper is/has been under review for the journal Atmospheric Measurement Techniques (AMT). Please refer to the corresponding final paper in AMT if available.

# Ash plume top height estimate using AATSR

T. H. Virtanen<sup>1</sup>, P. Kolmonen<sup>1</sup>, E. Rodríguez<sup>1</sup>, L. Sogacheva<sup>1</sup>, A.-M. Sundström<sup>2</sup>, and G. de Leeuw<sup>1,2</sup>

<sup>1</sup>Finnish Meteorological Institute, Erik Palmenin aukio 1, 00560 Helsinki, Finland

<sup>2</sup>Department of Physics, University of Helsinki, Gustav Hällströmin katu 2a, 00560 Helsinki, Finland

Received: 17 March 2014 – Accepted: 7 April 2014 – Published: 16 April 2014

Correspondence to: T. H. Virtanen (timo.h.virtanen@fmi.fi)

Published by Copernicus Publications on behalf of the European Geosciences Union.

Title Page

Abstract

Introduction

Conclusions

References

Tables

Figures

⏪

⏩

◀

▶

Back

Close

Full Screen / Esc

Printer-friendly Version

Interactive Discussion



## Abstract

An algorithm is presented for estimation of volcanic ash plume top height using the stereo view of the Advanced Along Track Scanning Radiometer (AATSR) aboard EN-VISAT. The algorithm is based on matching the top of atmosphere (TOA) reflectances and brightness temperatures of the nadir and 55° forward views, and using the resulting parallax to obtain the height estimate. Various retrieval parameters are discussed in detail, several quality parameters are introduced, and post-processing methods for screening out unreliable data have been developed. The method is compared against other satellite observations and in-situ data. The proposed algorithm is designed to be fully automatic, and can be implemented into operational retrieval algorithms. Combined with automated ash detection using the brightness temperature difference between the 11  $\mu\text{m}$  and 12  $\mu\text{m}$  channels, the algorithm allows simultaneous retrieval of horizontal and vertical dispersion of volcanic ash efficiently. A case study on the eruption of the Icelandic volcano Eyjafjallajökull in 2010 is presented. The height estimate method results are validated against available satellite and ground based data.

## 1 Introduction

Information on the dispersion of volcanic ash is important for air traffic safety, and satellite observations are the only way to obtain near real time (NRT) information on volcanic ash plumes on regional and global scales. Specialized satellite data products can be used by the airline industry and aviation authorities to avoid flying in areas affected by ash. In addition, the satellite observations are crucial for constraining ash dispersion models used for ash forecasts. While geostationary satellites with high temporal resolution are best suitable for near real time ash monitoring, the polar orbiting satellites can often provide more detailed information. In particular, the vertical profile of volcanic ash plumes can be studied using satellite based multiview instruments. Detailed stud-

# AMTD

7, 3863–3913, 2014

## Ash plume top height estimate using AATSR

T. H. Virtanen et al.

Title Page

Abstract

Introduction

Conclusions

References

Tables

Figures

◀

▶

◀

▶

Back

Close

Full Screen / Esc

Printer-friendly Version

Interactive Discussion



ies of the plume heights of past eruptions can help to understand the ash dispersion phenomena and to improve the dispersion models.

Height estimates based on multi-angle satellite data using stereo matching techniques have been used for decades. Early work by Hasler (1981) on satellite based stereo matching height estimates employed two geostationary satellites, and required manual matching of a pair of images. Since then, multiview satellite instruments have become available, and automatic image processing techniques have been developed. Prata and Turner (1997) introduced an algorithm for cloud-top height estimates using Along Tack Scanning Radiometer (ATSR) data. Their method is based on maximizing the cross correlation of nadir and forward views by allowing the forward view to be shifted. Muller et al. (2002) developed stereoscopic image matchers for the Multi-angle Imaging SpectroRadiometer (MISR), based on minimizing the difference between views, and Muller et al. (2007) describe a refined method for ATSR-2 data. Fisher et al. (2013) further developed these methods using AATSR data. The MISR height estimate methods have been applied to volcanic ash plumes e.g. by Scollo et al. (2012). Recently, Zakšek et al. (2013) proposed a method combining Spinning Enhanced Visible and InfraRed Imager (SEVIRI) and Moderate-resolution Imaging Spectroradiometer (MODIS) data.

Information on the ash plume height and thickness is also important for aerosol retrieval, in particular in estimating the ash concentrations. The satellite based instruments typically measure only the total aerosol load in an atmospheric column, without information on the aerosol profile or concentration. Information on the cloud thickness is needed in converting the satellite-retrieved column amounts [ $\text{g m}^{-2}$ ] to concentrations [ $\text{g m}^{-3}$ ]. The radiative transfer models often use rough guesses for the height and thickness of the aerosol layers, e.g. a homogeneous layer between 0–2 km might be assumed. This is usually adequate in the retrieval of the ambient aerosol optical depth (AOD) over broad areas with relatively low concentrations. The ash plumes, however, are distinct features having high contrast with the background, and highly varying heights in general. Thus information on the plume height may be of considerable impor-

## Ash plume top height estimate using AATSR

T. H. Virtanen et al.

Title Page

Abstract

Introduction

Conclusions

References

Tables

Figures



Back

Close

Full Screen / Esc

Printer-friendly Version

Interactive Discussion



tance to the ash load retrievals. Information on plume height and thickness that can be directly obtained from the stereo view geometry of AATSR is limited, but nevertheless valuable. Work on combining the AATSR dual view (ADV) aerosol retrieval algorithm (Kolmonen et al., 2013) with the AATSR correlation method (ACM) plume top height algorithm and automated ash detection is in progress. The aim is to simultaneously acquire information on the horizontal plume position and ash mass load, in addition to the plume height. The ash specific AOD retrieval will be discussed elsewhere.

In this article we describe an elevated feature height estimation algorithm for AATSR. Although our focus is on volcanic ash plumes, the method can in principle be used to estimate cloud top heights (CTH) or the height of any other feature, such as smoke and dust plumes or surface topography, provided that there is enough contrast in the measured top of atmosphere (TOA) reflectances or brightness temperatures. The ACM algorithm is largely based on existing methods. New aspects are that we allow a simultaneous across-track shift of the forward view, to compensate for across-track wind component. We also introduce and use several quality parameters based on statistical analyses, and allow simultaneous use of multiple correlation window sizes in the retrievals. New post-processing techniques to remove unreliable data are discussed as well. One of the key advantages in our approach is the automated ash detection using the brightness temperature difference method. The plume top heights are calculated for ash flagged pixels only, making the algorithm very efficient in processing large quantities of data.

From the available multiview instruments, AATSR is the optimal choice for ash plume height estimates. AATSR is unique in its ability to both detect volcanic ash using the thermal infrared (TIR) channels and to estimate the plume top height using the stereo view. In this paper we apply the height estimate algorithm to AATSR data only, although it is possible to apply it for MISR as well. Connection to ENVISAT was lost in April 2012, so the method presented here can only be applied to historical cases. The successor of AATSR, the Sea and Land Surface Temperature Radiometer (SLSTR) is scheduled

## Ash plume top height estimate using AATSR

T. H. Virtanen et al.

Title Page

Abstract

Introduction

Conclusions

References

Tables

Figures



Back

Close

Full Screen / Esc

Printer-friendly Version

Interactive Discussion



for launch in 2015. It has similar characteristics as AATSR (TIR channels and stereo view), and the method presented here can be applied to SLSTR data.

In Sect. 2, the area based correlation method algorithm for the estimation of volcanic ash plume top heights is described. In this method the correlation between brightness temperature data for the two views is optimized by shifting the forward view data in the along-track-direction. In Sect. 3 we show validation against available remote sensing and in-situ data as well as against surface height data. In Sect. 4 we apply the method the 2010 eruption of Eyjafjallajökull as a test case. Conclusions are given in Sect. 5.

## 2 Ash plume height estimate

Here we describe the characteristics of the AATSR instrument (Sect. 2.1), the ash detection technique (Sect. 2.2), the basic ideas behind the stereo view height estimate method (Sect. 2.3), and the AATSR correlation method (ACM) height estimate algorithm (Sect. 2.4). The height estimate results depend on several parameters used in the retrieval; these are discussed in Sect. 2.5. The primary product of ACM is the single pixel height, calculated for each ash flagged pixel separately. In addition, an averaged (smoothed) height product is provided, where the acceptance of pixels into the average is decided based on correlation method quality parameters and on statistical measures. This post processing is discussed in Sect. 2.6.

### 2.1 AATSR instrument

The AATSR instrument has seven channels centered at the wavelengths of 0.555, 0.659, 0.865, 1.61, 3.7, 10.85, and 12.0  $\mu\text{m}$ . The first four channels provide the ratio of reflected radiation to the incoming solar radiation at the top of the atmosphere, i.e. the TOA reflectance  $R$ , while the latter three channels provide information on the surface temperature via brightness temperatures  $T$ . The reflectance (visible) channels are used for the retrieval of aerosol properties using the ADV algorithm. The thermal infrared

## Ash plume top height estimate using AATSR

T. H. Virtanen et al.

Title Page

Abstract

Introduction

Conclusions

References

Tables

Figures



Back

Close

Full Screen / Esc

Printer-friendly Version

Interactive Discussion



(TIR) channels can be used for detection of the ash plumes, but also for retrieval of aerosol properties such as AOD, using alternative algorithms (de Leeuw et al., 2013). For the plume top height estimates we use the stereo view of AATSR: the instrument has a near nadir view and a 55° forward view. The two views are in principle collocated on the ground level. The plume height causes deviation from this in the direction along the satellite track, and the magnitude of the shift in this direction provides a way to estimate the plume height. Any of the channels can be used for the height estimate. The thermal infrared channels usually provide highest contrast of the ash plumes with the background, and the 10.85 μm channel is used by ACM as default. The horizontal resolution of AATSR is approximately 1 km.

## 2.2 Ash detection

A volcanic ash plume can be detected using the brightness temperatures difference (BTD) between two wavelengths, 11 μm and 12 μm (Prata, 1989). In first approximation, the brightness temperature difference  $BTD = T_{11} - T_{12}$  is negative for volcanic ash contaminated pixels, and positive for most other situations, such as meteorological clouds and clear sky scenes. The optimal BTD threshold for ash detected is not always exactly zero and e.g. water vapor tends to increase BTD, hiding the ash signal (Yu et al., 2002). Also, false alerts can be caused e.g. by desert dust or arctic haze. Although more detailed methods for ash detection exist for SEVIRI (Prata, 2013; Naeger et al., 2014) and for AIRS (Clarisse et al., 2010), for the purposes of this paper the simple BTD threshold method is sufficient.

## 2.3 Height estimate principle

The estimation of the ash plume top height is based on the stereo view of AATSR. The two AATSR views, a near-nadir and a ~ 55° forward view, are collocated on the ground level. At higher altitudes, the two views are looking at different positions (in the along-track direction), with the difference increasing with increasing height. Thus, for

## Ash plume top height estimate using AATSR

T. H. Virtanen et al.

Title Page

Abstract

Introduction

Conclusions

References

Tables

Figures

◀

▶

◀

▶

Back

Close

Full Screen / Esc

Printer-friendly Version

Interactive Discussion



an elevated feature with a detectable contrast to the background in both views, the height can be estimated by considering the apparent ground level difference in position between the two views (parallax).

A simplified illustration of the geometry is shown in Fig. 1. The cloud seems to be further away (with respect to the ground) in the forward view, as compared to the nadir view. The distance  $d$  between the projections of the cloud on Earth surface in the two views gets larger with increasing cloud height  $h$ . The simplified picture shows the geometry for sub-satellite track only, for which the nominal nadir and forward viewing angles are  $\mu_N = 0^\circ$  and  $\mu_F = 55^\circ$ , respectively, and the height is obtained from  $h = d / \tan 55^\circ$  (see Fig. 1). In the actual conical viewing geometry both viewing angles depend on the position of the pixel along the swath, and the height is obtained from  $h = d / (\tan \mu_F - \tan \mu_N)$ .

The height estimate process is automated by using a correlation method. The parallax is obtained by maximizing the correlation between the two views by allowing the forward view to be shifted. As a by-product, an estimate for the across-track wind can be obtained by allowing a two-dimensional shift, and taking into account the time gap of approximately 135 s between the two views.

The ACM height estimate is based on the gradients of the measured brightness temperatures (or other quantities) rather than the measured values themselves. If the measured quantities remain constant over large areas, the height cannot be estimated using the stereo view methods. It should also be noted that the total TOA radiation is used in the correlation procedure; for partially transparent plumes or clouds the method might not work. If there are surface features with high contrast below the plume, they may dominate the correlation.

## 2.4 Spatial correlation plume height estimate

We use an area-based cross correlation method, which compares a small nadir view image, called the nadir view correlation window (NCW), to a forward view image of the same size (forward view correlation window, FCW). The FCW is allowed to shift

## Ash plume top height estimate using AATSR

T. H. Virtanen et al.

Title Page

Abstract

Introduction

Conclusions

References

Tables

Figures



Back

Close

Full Screen / Esc

Printer-friendly Version

Interactive Discussion



## Ash plume top height estimate using AATSR

T. H. Virtanen et al.

Title Page

Abstract

Introduction

Conclusions

References

Tables

Figures

◀

▶

◀

▶

Back

Close

Full Screen / Esc

Printer-friendly Version

Interactive Discussion



pixel-by-pixel in both along-track and across-track directions, and the cross correlation coefficient  $C$  with the fixed-position NCW is calculated for each shift (Fig. 2). From the resulting correlation matrix, the forward view shift with highest correlation is selected, and it gives the cloud-top (or plume-top) collocation. While the along-track shift determines the height, the across-track wind speed component (at the plume top level) is obtained as a by-product from the across-track shift, taking into account the time gap of approximately two minutes between the two views. The known satellite-Earth geometry is used in converting the pixel shifts to height and wind speed estimates.

There are various alternative ways to define the cross correlation coefficient used in automatic height estimation. One of the first methods is described by Prata and Turner (1997), and is based on cross-correlating the measured data, normalized by RMS values:

$$C'(x, y; m, n) = \frac{\langle f_N(x, y) f_F(x + m, y + n) \rangle}{\sqrt{\langle f_N(x, y)^2 \rangle \langle f_F(x + m, y + n)^2 \rangle}}, \quad (1)$$

where  $f_N$  is the measured GBTR value (gridded brightness temperature or reflectance) in the nadir view, and  $f_F$  is the corresponding value in the forward view, with pixel shift  $(m, n)$  (in along-track  $(n)$  and across-track  $(m)$  directions, respectively). The coordinates  $x$  and  $y$  refer to the across-track (column) index and along-track (line) index, respectively (not to latitude or longitude). Here the average  $\langle \dots \rangle$  is defined (for both views respectively) as

$$\langle f(x, y) \rangle = \sum_{i=-M}^M \sum_{j=-N}^N f(x + i, y + j) / N_{\text{tot}}, \quad (2)$$

where the summation is over the correlation window (CW) and  $N_{\text{tot}}$  is the total number of pixels in the window. The index  $i$  runs through the across-track coordinate and the index  $j$  correspondingly through the along-track coordinate of the CW. The leading idea

## Ash plume top height estimate using AATSR

T. H. Virtanen et al.

Title Page

Abstract

Introduction

Conclusions

References

Tables

Figures

◀

▶

◀

▶

Back

Close

Full Screen / Esc

Printer-friendly Version

Interactive Discussion



in the correlation method height estimate is then that the highest coefficient  $C'$  among all shifts gives the best-fitting pixel shift  $(m, n)$ , and the corresponding height is the most probable plume top height. However, it turns out that using Eq. (1) leads to a lot of noise in the end results. There are many possible reasons for this, including different background atmospheric effects for nadir and forward views, and generally noise in the TOA satellite data. It may also happen that there is simply not enough contrast between the plume and the background. Fortunately, there are some statistical tricks to remove part of the background noise and improve the results.

The approach adopted here is to consider the deviation of the measured values from the local average, instead of the measured values themselves (Muller et al., 2007; Zakšek et al., 2013; Fisher et al., 2013). The cross correlation coefficient  $C$  at point  $(x, y)$  between the nadir and forward view data is defined as

$$C(m, n) = \frac{\langle (f_N - \mu_N)(f_F(m, n) - \mu_F(m, n)) \rangle}{\sigma_N \sigma_F(m, n) + \epsilon}, \quad (3)$$

where the forward view is shifted by  $m$  pixels in the across-track direction ( $x$ -axis) and  $n$  pixels in the along-track direction ( $y$ -axis). Here  $\epsilon$  is a small constant (0.001 by default) used for numerical stability and to avoid amplification of noise. Here we have dropped the coordinates  $x$  and  $y$  for notational brevity. The correlation coefficients are in the range  $-1 \leq C \leq 1$ . The average  $\mu_N = \langle f_N \rangle$  is defined as

$$\mu_N(x, y) = \sum_{i=-M}^M \sum_{j=-N}^N w_{i,j} f_N(x+i, y+j), \quad (4)$$

where the summation is over the correlation window (CW) of size  $N_{\text{tot}} = (2N + 1) \times (2M + 1)$ . The weight factor  $w_{i,j}$  can be based on the distance from the center point  $(x, y)$  for weighted average, or simply  $1/N_{\text{tot}}$  for arithmetic average. For the forward view average, nominally associated with point  $(x, y)$  but actually centered at the shifted

point  $(x + m, y + n)$ , we have

$$\mu_F(x, y, m, n) = \sum_{i=-M}^M \sum_{j=-N}^N w_{i,j} f_F(x + m + i, y + n + j). \quad (5)$$

This means that the whole forward view correlation window associated with  $(x, y)$  is shifted by vector  $(m, n)$ , as illustrated in Fig. 2. Naturally, the forward view average is different for each shift  $(m, n)$ . The allowed pixels shifts  $m$  and  $n$  are predefined,  $m \in \{-M_{\text{shift}}, \dots, M_{\text{shift}}\}$ ,  $n \in \{0, \dots, N_{\text{shift}}\}$  (only positive shifts are allowed for  $n$ , corresponding to positive heights).

The standard deviation  $\sigma$  is defined as

$$\sigma_N = \sqrt{\langle (f_N - \mu_N)^2 \rangle}, \quad \sigma_F = \sqrt{\langle (f_F - \mu_F)^2 \rangle}, \quad (6)$$

for both views, respectively. The averages are defined as above, with shift  $(m, n)$  implicitly assumed for the forward view.

The cross correlation coefficient is calculated for each pixel  $(x, y)$  and for each possible shift  $(m, n)$ . The shift corresponding to maximum  $C$  is selected as the best-fitting shift for the given pixel  $(x, y)$ . The height corresponding to this shift  $n$  is then calculated using appropriate Earth-satellite geometry. If  $\phi_1$  and  $\lambda_1$  correspond to the latitude and longitude of the original point  $(x, y)$  and  $\phi_2$  and  $\lambda_2$  correspond to the shifted point  $(x, y + n)$  (only along-track shift  $n$  is considered in the height estimate), the along-track distance  $d$  between these points can be approximated by

$$d = \sqrt{[\cos \phi_1 (\lambda_1 - \lambda_2)]^2 + (\phi_1 - \phi_2)^2} R_e, \quad (7)$$

where  $R_e = 6371.0$  km is the mean Earth radius. The pseudo-cartesian formula is adequate since we consider only short distances. The height is then obtained from

$$h = \frac{d}{\tan \mu_F - \tan \mu_N}. \quad (8)$$

## Ash plume top height estimate using AATSR

T. H. Virtanen et al.

Title Page

Abstract

Introduction

Conclusions

References

Tables

Figures

◀

▶

◀

▶

Back

Close

Full Screen / Esc

Printer-friendly Version

Interactive Discussion



## 2.5 Retrieval parameters

The ACM height estimate algorithm uses several parameters, which affect the results. These include the size of the correlation window, the maximum allowed shifts for the forward view (both along-track and across-track, in pixels), the BTD threshold used for ash detection, and the channel used in the correlation method. The primary retrieval parameters are listed in Table 1.

### 2.5.1 Brightness temperature difference

As already discussed, the threshold  $BTD < 0$  K used for ash detection is not necessarily the optimal value for all cases. Water vapor in the atmosphere increases the BTD, and thus a too low limit may cause that some ash contaminated areas are missed. On the other hand, some phenomena like arctic haze may cause small negative BTD values and cause false alerts. For consistency, the threshold of 0 K is systematically used in this study.

In addition to the initial ash detection, the way in which ash mask is used in the retrieval affects the results, particularly near the plume edges. The ash flags can be used in the correlation window: if a pixel in the window has its ash flag down, it may or may not be taken into account. If pixels from outside the plume are included, the resulting height may be lower than if non-ash pixels are excluded. On the other hand, if only ash flagged pixels are used in the correlation window, there may not be enough data for reliable results near the plume edges. In the present approach, the non-ash pixels are included in the correlation window.

### 2.5.2 Wavelength

The height estimate results depend on the choice of the channel used in the correlation method. In Fig. 3 we show full scene height estimates for two different channels, 555 nm and 10.85  $\mu\text{m}$ . The scene consists of an ash plume at (63° N, 18° W) extending to south-

## Ash plume top height estimate using AATSR

T. H. Virtanen et al.

Title Page

Abstract

Introduction

Conclusions

References

Tables

Figures



Back

Close

Full Screen / Esc

Printer-friendly Version

Interactive Discussion



## Ash plume top height estimate using AATSR

T. H. Virtanen et al.

Title Page

Abstract

Introduction

Conclusions

References

Tables

Figures

◀

▶

◀

▶

Back

Close

Full Screen / Esc

Printer-friendly Version

Interactive Discussion



east, high altitude meteorological clouds in the northern part, and open ocean and low level clouds. The 10.85  $\mu\text{m}$  channel is more sensitive to the water clouds, and the height estimate shows large elevated features in the northern part of the test scene. In particular, large parts of the water clouds on the northern part of the scene seem to lack sufficient contrast for the visible channel. The visible wavelength channel seems to detect only the thickest parts of the clouds, and gives a lower average height for the scene. The average height (standard deviation) is 2.71 (2.2) km for 10.85  $\mu\text{m}$ , and 2.06 (2.1) km for 555 nm. Both channels detect heights of 5–7 km for the ash plume, but the shape and other details differ.

Results obtained with the 12  $\mu\text{m}$  channel are similar to those obtained with the 10.85  $\mu\text{m}$  channel (not shown). The thermal channel centered at 10.85  $\mu\text{m}$  ( $T_{11}$ ) seems to be more sensitive for the ash plumes. For the results shown in this paper the 10.85  $\mu\text{m}$  channel has been used.

### 2.5.3 Correlation window size

The correlation window size (CWS) used in matching the two views can have a large effect on the results. A large window can detect large features but miss smaller ones, while a smaller window can create a lot of noise (Zakšek et al., 2013). Figure 4 shows retrievals made with three different CW sizes. The small  $5 \times 5$  CWS shown here contaminates the image with frequent high values. On the other hand, the large  $13 \times 13$  CWS blurs the image, and the plume edge heights, for example, are a mixture of the actual plume top and the surrounding ocean or lower cloud layer. Using large CWS leads to lower average plume heights, presumably due to contribution of the lower level features surrounding the plume.

The default CWS in ACM is  $11 \times 11$  pixels, but the algorithm calculates simultaneously two ancillary height estimates with smaller CWS,  $9 \times 9$  and  $7 \times 7$ . As output, the algorithm provides the height estimates for all three CWS and the standard deviation of the height between them. Currently, the algorithm uses rectangular correlation windows, and simple weights  $w_{i,j} = 1/N_{\text{tot}}$  in the correlation procedure, Eq. (4).

## 2.5.4 Allowed pixel shifts

The forward view correlation window is allowed to shift by  $m$  pixels in the across-track direction, and by  $n$  pixels in the along-track direction. The shifts are limited by conditions  $m \in \{-M_{\text{shift}}, M_{\text{shift}}\}$  and  $n \in \{0, N_{\text{shift}}\}$ . The along-track shift is limited to positive values, corresponding to positive heights. Increasing the maximum allowed shift  $N_{\text{shift}}$  leads to increase in the maximum height possible to be obtained by the algorithm. A large enough  $N_{\text{shift}}$  must be used so that the largest possible heights can be estimated reliably. Using unnecessarily large  $N_{\text{shift}}$  increases computation time, and may also result in erroneous, unrealistically high values. Extreme along-track shifts can be removed in post processing. In this work we use  $N_{\text{shift}} = 15$ , which corresponds to maximum height of approximately 12 km. Figure 5 shows how increasing  $N_{\text{shift}}$  affects the results.

The across-track shift does not directly affect the height, but it is important in adjusting to the temporal changes in the image pair, and to possible errors in the initial AATSR collocation. From Fig. 6 we see that if the across-track shift is not allowed, the height results would be very different. In this work the across-track shift is limited by  $M_{\text{shift}} = 5$ , which corresponds to maximum across-track wind components of approximately  $40 \text{ ms}^{-1}$ . For comparison, Zakšek et al. (2013) report maximum column shift of 20 pixels between two SEVIRI images, corresponding to approximately  $22 \text{ ms}^{-1}$ .

## 2.6 Post-processing

The single pixel height (SPH) values vary considerably from pixel to pixel, presumably due to effects related to the different viewing angles, and the time development of atmospheric features between the observations. To obtain more consistent results, we can use averaging over several pixels, and statistical filtering. The ACM algorithm produces data on two levels: first, a single pixel height (SPH) estimate is made for each ash-flagged pixel. Then, a moving average is calculated for each ash flagged pixel, using the SPH values of neighboring pixels. Only ash flagged pixels are accepted into the average, and quality filters can also be applied before averaging. At the same time,

## Ash plume top height estimate using AATSR

T. H. Virtanen et al.

Title Page

Abstract

Introduction

Conclusions

References

Tables

Figures



Back

Close

Full Screen / Esc

Printer-friendly Version

Interactive Discussion



we can calculate statistical variables related to the moving averaging window (MAW), and use those for further filtering. The resulting “best average height” (BAV) values are expected to be more representative than SPH data. However, the SPH data is also useful, since the quality filters often tend to remove a large portion of the original pixels.

Naturally, the average height results depend on the MAW size, possible weighting used in the averaging, and on the quality filters. In this section the effects of various parameters are discussed. The filtering parameters are listed in Table 2. Of course, the effectiveness of these parameters in improving the results can only be determined when reliable validation data is available. However, some conclusions can be made based on the variability of the heights; we expect the plume top heights to be rather uniform on horizontal scales of 10 km or so.

The first three parameters in Table 2, the correlation coefficient  $C$ , its standard deviation in the correlation matrix,  $\sigma_c$ , and the standard deviation of the along-track pixel shift with respect to the correlation window size,  $\sigma_{CWS}$ , are related to the principle of the correlation method. The next three parameters, standard deviation of height within the MAW  $\sigma_{av}$ , the standard deviation of the across-track shift within the MAW,  $\sigma_m$ , and the number of acceptable pixels  $n_{av}$  within the MAW, are related to the averaging. The three masks that can be applied to the SPH data are used to remove pixels where the algorithm chooses the maximum or zero along-track shift (extrema mask), pixels contaminated by water or ice clouds (cloud mask), or pixels where the forward view may be obstructed by a high feature earlier on the satellite track (shadow mask).

### 2.6.1 Averaging window size

In principle, there are two ways to do the averaging: increasing the pixel size, or using the moving averaging window (MAW) technique. The former would reduce the computational load, but is less flexible, so the latter method is used in the ACM algorithm. The averaged height is given in full resolution, i.e. a separate value is calculated for each pixel. Although technically the resolution remains the same, the averaging blurs

## Ash plume top height estimate using AATSR

T. H. Virtanen et al.

Title Page

Abstract

Introduction

Conclusions

References

Tables

Figures



Back

Close

Full Screen / Esc

Printer-friendly Version

Interactive Discussion



the details, as seen in Fig. 7. With an increasing MAW size the heights become more uniform, but less detailed.

Since the height estimate is based on integer pixel shifts in the along-track direction, the resulting data is quantized, i.e. the height distribution consists of a small number of distinct heights. This is partially smoothed when the pixel shifts are converted to heights, since the height depends on the latitude and on the position along the satellite swath. The averaging further smooths the data, hiding the initial quantized nature of the retrieval. Figure 7 illustrates the smoothing using a moving averaging window.

When calculating the average heights, the standard deviations of height ( $\sigma_{av}$ ) and across-track shift ( $\sigma_m$ ) within the MAW are also calculated. As discussed above, only ash-flagged pixels are used in the averaging, and some of the ash-flagged pixels within the MAW may be removed before the averaging by applying various thresholds. The number of acceptable pixels used in the average ( $n_{av}$ ) is recorded.

## 2.6.2 Cloud screening

The principle of the BTD threshold method for ash detection is simple: for volcanic ash  $BTD < 0$  and for water clouds  $BTD > 0$ . In practice, the situation is not that simple. The proper threshold is not always 0K, as it may depend on e.g. the water vapor content and the surface temperature. Since we concentrate on historic eruptions, the crude BTD threshold is usually sufficient for the present work. However, in mixed situations where thin water or ice clouds are situated above an ash plume, or when a thin ash plume lies above a lower cloud layer, the ACM algorithm may retrieve the height of the water/ice cloud layer, instead of the ash that causes negative BTD. Most of the usual cloud tests (Saunders et al., 1988; Koelemeijer et al., 2001) used in aerosol retrieval cannot be used in ash specific retrievals, since they tend to misidentify ash plumes as clouds. However, assuming that the water/ice clouds are brighter than the ash plumes, we can use a reflectance test at 659 nm to remove ash-flagged pixels with possible cloud contamination. The cloud test analyses one AATSR scene and automatically determines a reflectance threshold, above which the pixel is flagged cloudy (González,

## Ash plume top height estimate using AATSR

T. H. Virtanen et al.

Title Page

Abstract

Introduction

Conclusions

References

Tables

Figures



Back

Close

Full Screen / Esc

Printer-friendly Version

Interactive Discussion



2003). Figure 8 shows the effect of cloud mask on a test case. The RGB image of the scene (not shown) shows a water cloud layer below the ash plume around the central and southern parts of the plume.

The cloud mask can be applied to the data before averaging, but for many cases it is too stringent and removes most of the ash-flagged pixels. For the Eyjafjallajökull eruption the cloud mask removes on average more than 50 % of the ash-flagged pixels. The effect of the cloud screening is case dependent, and manual inspection of the images is often required for optimal results.

### 2.6.3 Shadow screening

At a given position along the satellite track, the forward view may be blocked by high plumes earlier on the track. The high features cast a “shadow”, the height of which decreases with distance. If the height of the “shadow” is higher than the height estimate given by the algorithm, the pixel is masked as “shadowed” (Fig. 9). The shadow mask is calculated from the initial single pixel height estimates. For the Eyjafjallajökull eruption, the shadow mask typically removes 10–30 % of the initial pixels.

## 2.7 Error characterization

Several assumptions are made in the height estimate method, and there are numerous sources of error. It is difficult to accurately quantify all the various error sources due to the nature of the correlation method. However, the quality parameters introduced in the previous section can be used to assess the contributions from different error sources to the height estimate.

### 2.7.1 Resolution

The nominal vertical resolution of the height estimate algorithm is approximately one kilometer, corresponding to a parallax of one pixel. We estimate a typical total error of 1–2 pixels, corresponding to 1–2 km in height. The default maximum shift in the along-

## Ash plume top height estimate using AATSR

T. H. Virtanen et al.

Title Page

Abstract

Introduction

Conclusions

References

Tables

Figures

⏪

⏩

◀

▶

Back

Close

Full Screen / Esc

Printer-friendly Version

Interactive Discussion



track direction is 15 pixels, so an error of 2 pixels corresponds to a relative uncertainty of 13–200 %, depending on the height.

The horizontal resolution (pixel size) is approximately one kilometer, with the exact value depending on latitude and on the position along the swath. The algorithm output contains height estimates in the full resolution. A moving average value over 25 (by default) neighboring pixels is also provided for each pixel, with the same nominal resolution.

## 2.7.2 Correlation method quality

The quality of the correlation method height estimate can be assessed using several quantities. First, the correlation coefficient  $C$  of each pixel is a natural measure of the quality of the estimate: for pixel with  $C$  approaching one we have high confidence in the reliability of the estimate, while pixels with  $C < 0.5$  are removed by default filters. Low values of  $C$  may occur due to many reasons. Large changes in the plume shape and position in the approximately 130 s time gap between the views is one possible cause for a low  $C$  value. Poor correlation can also be caused by effects due to differences in the viewing geometry; the forward view has a longer light path and is more affected by an ash layer. Also the underlying surface texture may have different relative contributions in the two views.

The second parameter that can be used in quality assessment is the standard deviation of the correlation coefficient,  $\sigma_c$  within the correlation window. If  $\sigma_c$  is low, i.e. if the amount of shift of the forward window does not make much difference, we cannot trust the results. This may happen for example if the scene considered is covered by a large cloud mass, with little or no high contrast features that could be matched between the two views. Another possible scenario where  $\sigma_c$  might be low is glinting sea surface, where any detectable features may be hidden in the noise.

## Ash plume top height estimate using AATSR

T. H. Virtanen et al.

Title Page

Abstract

Introduction

Conclusions

References

Tables

Figures



Back

Close

Full Screen / Esc

Printer-friendly Version

Interactive Discussion



### 2.7.3 Multilayer structures and transparency

Errors due to multilayer structures and transparent ash plumes are particularly difficult to quantify. The height estimate algorithm provides the height of the dominating feature in the scene, which may not necessarily be the ash plume, but e.g. an underlying water cloud or the ground surface. The correlation method relies on the assumption that the detected ash plume is the dominating feature in the scene, so that the algorithm can reliably track and collocate the plume features. However, if the ash plume is thin and transparent, the underlying surface texture may dominate the cross correlation. Thus the algorithm may not always find the plume top height, but the height of some other feature.

The noise seen in the initial single pixel height (SPH) data may be partly due to the algorithm jumping between the plume top level and surface or cloud level collocation. The variation of SPH within the MAW or between different CWS can be used as indicators of such jumping between features at different heights. The algorithm attempts to minimize the occurrence of such cases by applying thresholds to  $\sigma_{av}$  and  $\sigma_{CWS}$ .

### 2.7.4 Collocation

There is a known collocation error between the ground level nadir and forward views of AATSR (ESA, 2013) of two pixels in the along-track direction, and one pixel in the across-track direction (before the third reprocessing). This collocation error was independently observed when the ACM height estimate results were compared to topographic data, and a systematic correction is applied. However, it appears that the collocation is still not perfect, and artificial features (resembling the AATSR geometry) are seen in the height estimate results when applied to full AATSR swath (see Fig. 10d). In particular, the across-track shift data indicate that a further rectification of one pixel in the across-track direction would be necessary. The algorithm adjusts automatically in the across-track direction by allowing a shift of the forward view in this direction. The absolute value of the shift is not directly needed in calculating the height estimate, so

## Ash plume top height estimate using AATSR

T. H. Virtanen et al.

Title Page

Abstract

Introduction

Conclusions

References

Tables

Figures



Back

Close

Full Screen / Esc

Printer-friendly Version

Interactive Discussion



a systematic error in the across-track collocation is not critical. However, the across-track shift can be used to estimate the across-track wind component, which in turn can be used as a proxy for the along-track wind component, as discussed below.

### 2.7.5 Wind

5 An along-track wind component can cause an along-track shift of features between the forward and nadir view in the approximately two minute time gap between the forward and nadir overpasses (Prata and Turner, 1997). A best-fit parallax obtained by the correlation method can be caused partly by the height of the cloud and partly by its motion. Assuming that the parallax is due to height alone can cause a significant error.

10 An along-track wind speed component of approximately  $8 \text{ ms}^{-1}$  can cause a parallax of one pixel, or an error of  $\sim 1 \text{ km}$  in the height estimate.

The across-track shift obtained as a by-product in the height retrieval can be used as a qualitative indicator of possible errors due to along-track wind, if further information on the wind direction is available. As an example, a rough estimate of the wind speed can be made from Fig. 6. For the ash plume ( $\text{BTD} < 0$ ) the average shift is 1.5 pixels, corresponding roughly to  $11 \text{ ms}^{-1}$  wind speed. From the direction of the ash plume relative to the swath, we can estimate that the along-track component is roughly one third of this, i.e. smaller than  $4 \text{ ms}^{-1}$ . This corresponds to an along-track shift of less than a pixel, and thus it is not likely that the along-track wind causes very large error in the height estimate in this case. In general, if we assume the along and across-track wind components to be equal, the typical across-track shift of one pixel indicates an uncertainty of  $\sim 1 \text{ km}$  in the height.

The ash plume may also change its shape and altitude between the two observations. Prata and Turner (1997) argue that the vertical updraft as such is not a major source of error, since the height information is essentially obtained at the time of the forward overpass. Also, since the correlation window size is typically of the order of  $10 \text{ km}^2$ , modest changes in the cloud morphology should not have a large effect on the height estimate.

## Ash plume top height estimate using AATSR

T. H. Virtanen et al.

Title Page

Abstract

Introduction

Conclusions

References

Tables

Figures



Back

Close

Full Screen / Esc

Printer-friendly Version

Interactive Discussion



### 3 Validation and comparisons

The height estimates should be validated against independent in-situ sources, and compared against available remote sensing data. In this section we compare the ACM height estimates to five independent sources. Since the algorithm can be used to estimate the height of any elevated feature, including ground surface, we can verify the method principle against surface topography data. We also use two satellite based instruments, MISR and CALIOP, for comparison. In addition, we use data from two ground based sources for the Eyjafjallajökull eruption, the Keflavik weather radar and a database derived from web camera imagery.

#### 3.1 Topography

Comparison against topographic data is the best way to validate the principle of the algorithm. Accurate information on the surface height is available globally at high resolution and without the need to consider timing. The errors in validation data are negligible considering the nominal resolution of 1 km of the height estimate.

The ACM algorithm aims at providing height estimates for elevated atmospheric features such as clouds and ash plumes, and thus validation against ground targets is not sufficient. While the cloud-free ground surface is opaque, offering an ideal target for the correlation method, clouds and plumes can be partially transparent and have a complicated three-dimensional structure with multilayer features. However, the overwhelming availability and quality of the topographic data is valuable for testing the basic principles of the height estimate method.

For this test case we have chosen an almost cloud free scene over the Himalayas on 4 May 2010 at 04:19, AATSR orbit ATS\_TOA\_1PRUPA20100504\_041906. The surface heights are obtained from [http://topex.ucsd.edu/cgi-bin/get\\_data.cgi/](http://topex.ucsd.edu/cgi-bin/get_data.cgi/). The area has sufficient contrast in both surface reflectivity and brightness temperatures for the tests to work, in principle: the mountain tops are cold and snow covered, while the surrounding terrain has darker surfaces and higher temperatures. Although we searched

## Ash plume top height estimate using AATSR

T. H. Virtanen et al.

Title Page

Abstract

Introduction

Conclusions

References

Tables

Figures



Back

Close

Full Screen / Esc

Printer-friendly Version

Interactive Discussion



for least possible cloud cover, some uncertainty is still caused by cloud contamination. The difficulty is that the standard cloud tests mask the mountain tops as cloudy, since they are bright and cold, and it is difficult to distinguish between the actual clouds (which are a nuisance here) and the mountain tops (which we are studying).

In the comparison we use the AATSR grid and average the high resolution surface topography data around each AATSR pixel. The per pixel comparison shows excellent agreement between the ACM height estimate and the surface height data, considering that some cloud contamination is present (Fig. 10). The scatter plot in Fig. 10f shows fair overall agreement, with correlation coefficient 0.96. Cloud contamination can be seen in the scatter plot as peaks in the ACM data. Some of the features of the mountain range are captured by ACM, but most details are blurred by noise in the ACM data. The crosscut height profile in Fig. 10e shows the agreement between ACM and topography data, and also illustrates the ACM vertical resolution of approximately one kilometer. The ACM algorithm shows slight overestimation of heights on the southern edge of the mountain range. This may be due to cloud contamination, but it may be also related to the AATSR viewing geometry: the southern slope is facing “away” from the forward view of AATSR, moving from north to south. A surface shadow mask was not applied to the ACM data, although the AATSR forward view may be obstructed by some of the steep slopes.

### 3.2 MISR

MISR, with its nine views, is an optimal instrument for height estimates of atmospheric features. Unfortunately, for our purposes it has limited usability due to its lack of TIR channels for ash detection. However, it provides useful comparison data for the ACM height estimates. There is a number of M-series height estimate algorithms and various tools for cloud top height estimates (Muller et al., 2002, 2007; Fisher et al., 2013). Particularly interesting for our work is the MISR Plume Height Project (NASA, 2013), where the height estimates are calculated for some manually selected ash plumes.

## Ash plume top height estimate using AATSR

T. H. Virtanen et al.

Title Page

Abstract

Introduction

Conclusions

References

Tables

Figures



Back

Close

Full Screen / Esc

Printer-friendly Version

Interactive Discussion



In the following we compare the height estimates made with the AATSR correlation method (ACM) to the MISR plume height project (MPHP) height estimates.

In Table 3 we show the average heights (and standard deviation of height) for both AATSR and MISR data for the eight cases where overlapping data exists. In the comparison only common pixels have been used, i.e. data is limited by both the MPHP hand-made plume polygon and by the AATSR BTD  $< 0$  K threshold. We have used the MPHP grid, and averaged the ACM data within 4 km radius from the grid point. The number of common MPHP pixels  $N$  is given in the table. The pixel-by-pixel correlation coefficients  $R$  are also given for each case, and we see that the correlation is poor. This is not surprising, given that there is a time gap of approximately two hours between the overpasses, during which the plumes may have shifted. The averaged plume heights are a better starting point for the comparison, but some collocation and ash identification issues remain. For example, the common pixels (those that pass the AATSR BTD  $< 0$  K thresholds and are within the MPHP polygon) may not give representative subsets of the plume height data. A more reasonable comparison might be achieved by manually selecting corresponding plume areas from both data, taking into account the horizontal motion of the plume during the time lapse, but such selection is prone to interpretation bias, and is not conducted here.

In Table 3 we give the averaged heights for the original data and for the common pixels, respectively. The heights averaged over common pixels are similar for all cases, except the first one on 15 April. For this case, the MPHP plume polygon is not strictly limited to the ash plume, but contains surrounding sea surface areas as well. This is seen as the much smaller average height than for ACM in the comparison.

In Fig. 11 we show MPHP and ACM data, and their comparison, for an Eyjafjallajökull ash plume just south of Iceland on 16 May 2010. For AATSR, we use the single pixel heights (SPH); comparison with the best average height (BAV) data gives only slightly improved results. For the test case data, limited by both the MPHP plume area and by the AATSR BTD threshold, the average height (standard deviation) is 6.1 (0.57) km for MPHP and 5.5 (1.15) km for ACM. Although the heights averaged over the whole

## Ash plume top height estimate using AATSR

T. H. Virtanen et al.

Title Page

Abstract

Introduction

Conclusions

References

Tables

Figures



Back

Close

Full Screen / Esc

Printer-friendly Version

Interactive Discussion



plume are not too different, the pixel-by-pixel scatter plot shows poor agreement. Part of this can be explained by the  $\sim 2$  h time gap between the overpasses; from the RGB images (not shown) we can clearly see that the plume has shifted to the north between the AATSR and MISR images, which is not taken into account in the scatter plot. We see that the MISR results show rather uniform heights, whereas much more variation is seen in the AATSR data.

There are several differences in acquisition of the two data sets. Although the correlation algorithms are based on the same principles, there are differences in the normalization procedures, correlation window sizes and other retrieval parameters. The MPHP data is obtained using a visible wavelength channel (671 nm), while for AATSR we use a TIR channel (10.85  $\mu\text{m}$ ). Also, for the MISR data smaller viewing zenith angles (VZA) are used: MPHP typically uses 6 of the oblique cameras, labeled A (26.1°), B (45.6°) and C (60.0°), paired with the nadir view camera for in the correlation method. A lower VZA leads to lower vertical resolution, and thus to more uniform plume heights for MPHP data. On the other hand, a larger VZA leads to increasing differences in the viewing geometry, and increasing errors due to plume shadowing and different light path lengths. There are wind corrected height estimates available for the MISR data, but in the comparison we have used only data without wind correction.

### 3.3 CALIOP

The lidar data from the Cloud–Aerosol Lidar with Orthogonal Polarization (CALIOP) on the Cloud–Aerosol Lidar and Infrared Pathfinder Satellite Observations (CALIPSO) platform (Winker et al., 2007) gives accurate ash plume heights, but with its limited coverage it is difficult to find even remotely simultaneous overpasses with AATSR, where ash is present. One such case is found South-West of Iceland, where a large ash cloud is observed by AATSR on 7 May 2010 at 22:51 (all times in this article are given in UTC). The plume is crossed by CALIPSO some five hours later on 8 May 2010 at 04:04. From hourly SEVIRI data (Prata and Prata, 2012; Prata, 2013) between 23:00 7 May and 04:00 8 May we see that the ash plume, which initially coincides with the

## Ash plume top height estimate using AATSR

T. H. Virtanen et al.

Title Page

Abstract

Introduction

Conclusions

References

Tables

Figures

◀

▶

◀

▶

Back

Close

Full Screen / Esc

Printer-friendly Version

Interactive Discussion



plume observed by AATSR, moves south by approximately two degrees in five hours (Fig. 12). Considering this, there is remarkable agreement between the ACM height estimate and the CALIOP sounding.

The CALIOP data shows three thicker ash layers approximately at 10, 7.5 and 5 km heights, and ACM shows data at similar altitudes. There are also lower level cloud structures at  $\sim 3$  and  $\sim 1$  km levels, which are picked by ACM on the edges of the plume. It is possible that the vertical structure of the plume is changed in the five hours between the observations, but the smooth transition of the plume with only modest changes in the horizontal shape (as observed in the six hourly SEVIRI images) imply that drastic changes have not necessarily occurred. A few other similar cases of near simultaneous overpasses can be found, with decent agreement between the data but with some collocation issues remaining.

### 3.4 Weather radar and webcam

Ground based plume top height data for Eyjafjallajökull includes Keflavík weather radar plume top height estimates and time series of plume top altitudes constructed from web camera images (Arason et al., 2011). These data give one height value for each time, for the maximum plume top height over the volcano. From all the AATSR ash plume cases for the Eyjafjallajökull eruption, only 13 have data over the volcano, six in day-time and seven cases in the night time retrievals. In Fig. 13 we compare the ACM data, averaged over all ash-flagged pixels within 50 km from the volcano, with the radar and web camera data. Generally the ACM heights follow the in-situ data well, considering that the averaging smooths the somewhat noisy ACM single pixel height data. Note that the weather radar data has a minimum height of 2.5 km and the web camera data has a maximum height of 5.2 km a.s.l. at the volcano.

## Ash plume top height estimate using AATSR

T. H. Virtanen et al.

Title Page

Abstract

Introduction

Conclusions

References

Tables

Figures



Back

Close

Full Screen / Esc

Printer-friendly Version

Interactive Discussion



## 4 Case study: Eyjafjallajökull

As an example, we apply the AATSR correlation method height estimate algorithm to the Icelandic Eyjafjallajökull eruption in 2010. The course of eruption and ash dispersal is described e.g. by Gudmundsson et al. (2012). Ash detection and mass load retrieval by SEVIRI for the eruption period is described by Prata and Prata (2012), and a detailed dispersion model study, including plume height information, is presented by Stohl et al. (2011). Volcanic ash plume top heights for several days in April during the eruption are estimated using combined SEVIRI and MODIS data by Zakšek et al. (2013). The eruption can be divided into three periods: in the first phase (14–17 April) ash was spread to South-East over Northern and Central Europe; in the second phase (18 April–4 May) less ash was produced and it was only observed near Iceland; in the third phase (5–18 May) the eruption intensity increased again, and ash was dispersed in all directions and over large distances.

For the first phase of the eruption we have data on three days. On 15 April a narrow plume is observed near the Faroe Islands at 3–5 hm height, extending from West to East. On 16 April two distant ash clouds were observed over Poland with heights of around 4 km and 1 km, respectively. For the second eruption phase we have no AATSR observations with the  $BTD < 0\text{ K}$  threshold. However, this lack of detected ash is partly due to the threshold being too strict for the steam-rich plumes, rather than due to absence of ash. The water vapor within the ash plume tends to increase BTM, thus preventing the detection with  $0\text{ K}$  threshold. In the third phase of the eruption we observe several large ash plumes and clouds in all directions around Iceland. In Fig. 14 we show the height estimate for four days during the latter part of the eruption. The figure also illustrates the typical AATSR swaths near Iceland; the AATSR revisit time is approximately three days, and even large plumes may be missed in the gaps between the orbits.

Using the  $BTD < 0\text{ K}$  threshold, we have searched for day time ash plumes in the period from 15 April to 18 May 2010, in an area between  $40^\circ\text{ W}$ ,  $35^\circ\text{ E}$  and  $40^\circ\text{ N}$ ,  $80^\circ\text{ N}$ .

AMTD

7, 3863–3913, 2014

### Ash plume top height estimate using AATSR

T. H. Virtanen et al.

Title Page

Abstract

Introduction

Conclusions

References

Tables

Figures

◀

▶

◀

▶

Back

Close

Full Screen / Esc

Printer-friendly Version

Interactive Discussion



## Ash plume top height estimate using AATSR

T. H. Virtanen et al.

Title Page

Abstract

Introduction

Conclusions

References

Tables

Figures



Back

Close

Full Screen / Esc

Printer-friendly Version

Interactive Discussion



Ash was detected on 25 AATSR orbits, for 17 different days. In night time retrievals 18 additional ash-affected orbits were found, on 15 different days. Days where the 0 K threshold showed only a limited number of isolated ash-flagged pixels were interpreted as false alerts and removed from the analysis. Although some clouds detected by the 0 K threshold may be false alerts, like the low-level cloud over Greenland on 6 May seen in Fig. 14a, all ash flagged pixels are included in the analysis for the days considered for consistency.

In Table 4 we show statistics for the full eruption period for day time orbits. The night time retrievals differ for example in the cloud screening, and they are not included in this analysis. For each day with data we list the number of ash flagged pixels ( $N$ ), the number of pixels after filtering ( $N_{\text{bav}}$ ), the fraction of the filtered (best average height) pixel from the total (bav frac.), the fraction of cloud flagged pixels (Cld frac.), the fraction of pixels where the forward view is obscured (Shd frac.), and the fraction of pixels where the ACM algorithm selects zero or maximum pixel shift (Ext frac.). Four daily average height values (km a.s.l.) are also given: the daily average of filtered pixel heights (BAV), and the average single pixel heights with the largest CW (SPH), medium size CW (MwH) and the small CW (SwH). In Fig. 15 we show a time series of the daily average plume top heights and number of ash flagged pixels. Typically, the smaller correlation window gives larger average heights, with more variation. The average BAV heights are lower or higher than the SPH heights, depending on the case. On average, the filtering removes more than 80 % of the pixels, mostly because of cloud screening. It is evident that the use of systematic thresholds for all cases leads to a large fraction of the pixels being removed, while the obtained improvement in reliability is uncertain. Instead, possible thresholds and filters should be considered case by case. More abundant, reliable, reference data is needed.

As a more detailed example, we study the case of 6 May 2010 over Iceland in Fig. 16. In this case, the AATSR overpass is directly over the volcano, and a large plume extends from the volcano first directly to east, and then turns to south. The wind direction is captured by the across-track wind speed estimate retrieved by ACM, Fig. 16e: posi-

tive values in the northern part of the plume indicate eastward (or southeastward) wind, while the values close to zero in the southern part correspond to a zero across-track wind component. The BTD values are smallest in the middle of the plume in this case (Fig. 16f), but this is not a general rule.

5 The height reaches 10 km in the eastward plume, while the southern tip of the plume is below 5 km, with an average height around 5.6 km for the whole plume (Fig. 16a). The BAV heights (Fig. 16b) are similar to the SPH values, with less remaining data points. The standard deviation of BAV data is slightly smaller than for the SPH data, but the average height remains nearly the same. Lower quality pixels are removed mostly from  
10 the plume edges, but also from the central parts of the plume. For this example we have turned the cloud mask off, as it removes 65 % of the plume. The gap in the height estimate data around 61.8° N is due to an AATSR scene edge. ACM requires margins around each scene, which results in gaps between the scenes (a technical problem to be addressed in future versions).

15 The correlation coefficient  $C$  values range mostly from 0.5 to 0.95, with an average of 0.87 and 0.89 median (Fig. 16d). There is spatial variability in  $C$ , with standard deviation of 0.08. The standard deviation of  $C$  within the correlation matrix  $\sigma_c$  has most of its values between 0.1 and 0.6, with a 0.28 average, 0.27 median, and 0.11 standard deviation (within MAW). The highest  $\sigma_c$  values are typically on the central parts of  
20 the plume, and the lowest values are on the plume edges (Fig. 16c). There are no large areas where the correlation method quality parameters  $C$  and  $\sigma_c$  would clearly indicate lower quality of the height estimate; hence it appears that the estimate quality cannot be easily improved by applying thresholds to these parameters. For a better understanding of the use of these parameters as quality indicators on a single pixel  
25 bases would require more abundant and reliable reference data.

**Ash plume top height estimate using AATSR**

T. H. Virtanen et al.

Title Page

Abstract

Introduction

Conclusions

References

Tables

Figures



Back

Close

Full Screen / Esc

Printer-friendly Version

Interactive Discussion



## 5 Conclusions

We have developed a height estimate algorithm based on cross correlation of AATSR nadir and forward view image pairs. The AATSR correlation method algorithm has been validated against topographic data and compared against other satellite based instruments and in-situ data, and is shown to perform reasonably well. Using the algorithm and automatic ash detection based on the thermal infrared channels of AATSR, we have studied the volcanic ash plume top heights of the Eyjafjallajökull eruption in Iceland in April and May 2010.

Sensitivity of the method to various retrieval parameters is discussed in detail. An attempt is made to take into account various error sources and filter the data by quality thresholds. However, the results are inconclusive, and suitable thresholds vary from case to case. For best result, the useful quality parameter thresholds need to be manually tuned for each case.

The data are made available via the VAST project web page, <http://vast.nilu.no/>. See also the publicly available ATBD of AATSR plume heights (Virtanen and de Leeuw, 2013).

*Acknowledgements.* This work was supported by the Centre of Excellence in Atmospheric Science funded by the Finnish Academy of Sciences (project no. 272041), and the European Space Agency through the project Volcanic Ash Strategic initiative Team (VAST, ESA-ESRIN Contract No. 4000105701/12/I-LG). The AATSR data were obtained from ESA. The CALIOPS data were obtained through NASA Langley Research Center website (<http://www-calipso.larc.nasa.gov/>). The MISR data were obtained via the online archive of MISR Plume Height Project (<http://misr.jpl.nasa.gov/getData/accessData/MisrMinxPlumes/>). SEVIRI data were obtained through the VAST database, courtesy of F. Prata. The Keflavík weather radar data and the web camera data published by Arason et al. (2011) were obtained through the VAST database.

## Ash plume top height estimate using AATSR

T. H. Virtanen et al.

Title Page

Abstract

Introduction

Conclusions

References

Tables

Figures



Back

Close

Full Screen / Esc

Printer-friendly Version

Interactive Discussion



## References

- AATSR 3rd Reprocessing User Note, Issue 1.0, European Space Agency: ESA AATSR internet site, available at: <https://earth.esa.int/web/guest/missions/esa-operational-eo-missions/envisat/instruments/aatsr> (last access: 14 April 2014), 2013. 3880
- 5 Arason, P., Petersen, G. N., and Björnsson, H.: Observations of the altitude of the volcanic plume during the eruption of Eyjafjallajökull, April–May 2010, *Earth Syst. Sci. Data*, 3, 9–17, doi:10.5194/essd-3-9-2011, 2011. 3886, 3890, 3910
- Clarisse, L., Prata, A. J., Lacour, J.-L., Hurtmans, D., Clerbaux, C., and Coheur, P.-F.: A correlation method for volcanic ash detection using hyperspectral infrared measurements, *Geophys. Res. Lett.*, 37, L19806, doi:10.1029/2010GL04448, 2010. 3868
- 10 Curier, L., de Leeuw, G., Kolmonen, P., Sundström, A.-M., Sogacheva, L., and Bennouna, Y.: Aerosol retrieval over land using the (A)ATSR dual-view algorithm, in: *Satellite Aerosol Remote Sensing Over Land*, edited by: Kokhanovsky, A. A. and de Leeuw, G., Springer, Berlin, 2009.
- 15 de Leeuw, G., Holzer-Popp, T., Bevan, S., Davies, W., Desclotres, J., Grainger, R. G., Griesfeller, J., Heckel, A., Kinne, S., Klüser, L., Kolmonen, P., Litvinov, P., Martynenko, D., North, P. J. R., Ovigneur, B., Pascal, N., Poulsen, C., Ramon, D., Schulz, M., Siddans, R., Sogacheva, L., Tanré, D., Thomas, G. E., Virtanen, T. H., von Hoyningen Huene, W., Vountas, M., and Pinnock, S.: Evaluation of seven European aerosol optical depth retrieval algorithms for climate analysis, *Remote Sens. Environ.*, doi:10.1016/j.rse.2013.04.023, in press, 2013. 3868
- 20 Fisher, D., Muller, J.-P., and Yershov, V. N.: Automated stereo retrieval of smoke plume injection heights and retrieval of smoke plume masks from AATSR and their assessment with CALIPSO and MISR, *IEEE T. Geosci. Remote*, 52, 1249–1258, doi:10.1109/TGRS.2013.2249073, 2013. 3865, 3871, 3883
- 25 Gudmundsson, M. T., Thordarson, T., Höskuldsson, A., Larsen, G., Björnsson, H., Prata, A. J., Oddsson, B., Magnússon, E., Högnadóttir, T., Petersen, G. N., Hayward, C. L., Stevenson, J. A., and Jónsdóttir, I.: Ash generation and distribution from the April–May 2010 eruption of Eyjafjallajökull, Iceland, *Sci. Rep.*, 2, 572, doi:10.1038/srep00572, 2012. 3887
- 30 Hasler, A. F.: Stereographic observations from geosynchronous satellites: an important new tool for the atmospheric sciences, *B. Am. Meteorol. Soc.*, 62, 194–212, 1981. 3865

### Ash plume top height estimate using AATSR

T. H. Virtanen et al.

Title Page

Abstract

Introduction

Conclusions

References

Tables

Figures

⏪

⏩

◀

▶

Back

Close

Full Screen / Esc

Printer-friendly Version

Interactive Discussion



## Ash plume top height estimate using AATSR

T. H. Virtanen et al.

Title Page

Abstract

Introduction

Conclusions

References

Tables

Figures

◀

▶

◀

▶

Back

Close

Full Screen / Esc

Printer-friendly Version

Interactive Discussion

- Koelemeijer, R. B. A., Stammes, P., Hovenier, J. W., and de Haan, J. D.: A fast method for retrieval of cloud parameters using oxygen A-band measurements from the Global Ozone Monitoring Instrument, *J. Geophys. Res.*, 106, 3475–3490, 2001. 3877
- 5 Kolmonen, P., Sundström, A.-M., Sogacheva, L., Rodriguez, E., Virtanen, T., and de Leeuw, G.: Uncertainty characterization of AOD for the AATSR dual and single view retrieval algorithms, *Atmos. Meas. Tech. Discuss.*, 6, 4039–4075, doi:10.5194/amtd-6-4039-2013, 2013. 3866
- Muller, J.-P., Mandanayake, A., Moroney, C., Davies, R., Diner, D. J., and Paradise, S.: MISR Stereoscopic Image Matchers: techniques and results, *IEEE T. Geosci. Remote*, 40, 1547–1559, doi:10.1109/TGRS.2002.801160, 2002. 3865, 3883
- 10 Muller, J.-P., Denis, M.-A., Dundas, R. D., Mitchell, K. L., Naud, C., and Mannstein, H.: Stereo cloud-top heights and cloud fraction retrieval from ATSR-2, *Int. J. Remote Sens.*, 28, 1921–1938, doi:10.1080/01431160601030975, 2007. 3865, 3871, 3883
- Naeger, A. R. and Christopher, S. A.: The identification and tracking of volcanic ash using the Meteosat Second Generation (MSG) Spinning Enhanced Visible and Infrared Imager (SEVIRI), *Atmos. Meas. Tech.*, 7, 581–597, doi:10.5194/amt-7-581-2014, 2014. 3868
- 15 NASA: JPL MISR plume height project webpage, available at: <http://www-misr.jpl.nasa.gov/getData/accessData/MisrMinxPlumes> (last access: 14 April 2014), 2013. 3883
- Prata, A. J.: Radiative transfer calculations for volcanic ash clouds, *Geophys. Res. Lett.*, 16, 1293–1296, 1989. 3868
- 20 Prata, A. J.: Detecting and Retrieving Volcanic Ash from SEVIRI Measurements Algorithm Theoretical Basis Document v1.0, ESA/VAST, Kjeller, 67 pp., available at: <http://vast.nilu.no/project/deliverables/>, 2013. 3868, 3885
- Prata, A. J. and Prata, A. T.: Eyjafjallajökull volcanic ash concentrations determined using Spin Enhanced Visible and Infrared Imager measurements, *J. Geophys. Res.*, 117, D00U23, doi:10.1029/2011JD016800, 2012. 3885, 3887
- 25 Prata, A. J. and Turner, P. J.: Cloud-top height determination using ATSR data, *Remote Sens. Environ.*, 59, 1–13, 1997. 3865, 3870, 3881
- Robles González, C.: Retrieval of Aerosol Properties Using ATSR-2 Observations and Their Interpretation, Ph.D. thesis, University of Utrecht, Utrecht, the Netherlands, 2003. 3877
- 30 Saunders, R. W. and Kriebel, K. T.: An improved method for detecting clear sky and cloudy radiances from AVHRR data, *Int. J. Remote Sens.*, 9, 123–150, 1988. 3877

## Ash plume top height estimate using AATSR

T. H. Virtanen et al.

Title Page

Abstract

Introduction

Conclusions

References

Tables

Figures

◀

▶

◀

▶

Back

Close

Full Screen / Esc

Printer-friendly Version

Interactive Discussion



Scollo, S., Kahn, R. A., Nelson, D. L., Coltelli, M., Diner, D. J., Garay, M. J., and Realmuto, V. J.: MISR observations of Etna volcanic plumes, *J. Geophys. Res.*, 117, D06210, doi:10.1029/2011JD016625, 2012. 3865

5 Stohl, A., Prata, A. J., Eckhardt, S., Clarisse, L., Durant, A., Henne, S., Kristiansen, N. I., Minikin, A., Schumann, U., Seibert, P., Stebel, K., Thomas, H. E., Thorsteinsson, T., Tørseth, K., and Weinzierl, B.: Determination of time- and height-resolved volcanic ash emissions and their use for quantitative ash dispersion modeling: the 2010 Eyjafjallajökull eruption, *Atmos. Chem. Phys.*, 11, 4333–4351, doi:10.5194/acp-11-4333-2011, 2011. 3887

10 Virtanen, T. H. and de Leeuw, G.: Volcanic ash plume top height estimate using AATSR algorithm theoretical basis document v1.0, ESA/VAST, Helsinki, 35 pp., available at: <http://vast.nilu.no/project/deliverables/>, 2013. 3890

Winker, D. M., Hunt, W. H., and McGill, M. J.: Initial performance assessment of CALIOP, *Geophys. Res. Lett.*, 34, L19803, doi:10.1029/2007GL030135, 2007. 3885

15 Yu, T., Rose, W. I., and Prata, A. J., Atmospheric correction for satellite-based volcanic ash mapping and retrievals using “split window” IR data from GOES and AVHRR, *J. Geophys. Res.*, 107, 4311, doi:10.1029/2001JD000706, 2002. 3868

20 Zakšek, K., Hort, M., Zaletelj, J., and Langmann, B.: Monitoring volcanic ash cloud top height through simultaneous retrieval of optical data from polar orbiting and geostationary satellites, *Atmos. Chem. Phys.*, 13, 2589–2606, doi:10.5194/acp-13-2589-2013, 2013. 3865, 3871, 3874, 3875, 3887

## AMTD

7, 3863–3913, 2014

## Ash plume top height estimate using AATSR

T. H. Virtanen et al.

**Table 1.** Retrieval parameters, which need to be set prior to each retrieval. The default values are used in the results shown in this paper, unless otherwise indicated.

Abbreviation	Description	Default
BTD	BTD = $T_{11} - T_{12}$ threshold	0 K
CWS	Correlation window size	11 × 11
$N_{\text{shift}}$	Maximum along-track shift	15
$\pm M_{\text{shift}}$	Maximum across-track shift	5
Channel	Channel used in the retrieval	$T_{11}$

Title Page

Abstract

Introduction

Conclusions

References

Tables

Figures

◀

▶

◀

▶

Back

Close

Full Screen / Esc

Printer-friendly Version

Interactive Discussion



## Ash plume top height estimate using AATSR

T. H. Virtanen et al.

**Table 2.** Parameters that can be used for filtering the height estimate data, and the default values. In the ACM output, both the original unfiltered single pixel heights and the filtered MAW-averaged heights are given. See text for details.

Parameter	Usage	Default threshold
$C$	$C > C^{\text{lim}}$	0.5
$\sigma_c$	$\sigma_c > \sigma_c^{\text{lim}}$	0.15
$\sigma_{\text{CWS}}$	$\sigma_{\text{CWS}} < \sigma_{\text{CWS}}^{\text{lim}}$	20
$\sigma_{\text{av}}$	$\sigma_{\text{av}} < \sigma_{\text{av}}^{\text{lim}}$	3.0
$\sigma_m$	$\sigma_m < \sigma_m^{\text{lim}}$	3
$n_{\text{av}}$	$n > n_{\text{av}}$	4
extrema	on/off	On
shadow	on/off	On
cloud	on/off	On

Title Page

Abstract

Introduction

Conclusions

References

Tables

Figures

◀

▶

◀

▶

Back

Close

Full Screen / Esc

Printer-friendly Version

Interactive Discussion



## Ash plume top height estimate using AATSR

T. H. Virtanen et al.

**Table 3.** Number of the common pixels ( $N$ ) for the MPHP and ACM data, the corresponding average heights for the full original plumes (orig) and for common pixels only (comm), and the correlation coefficient  $R$ . Only the single pixel height (SPH) values for ACM are shown here.

Date	$N$	$h_{\text{acm}}^{\text{orig}}$	$h_{\text{mphp}}^{\text{orig}}$	$h_{\text{acm}}^{\text{comm}}$	$h_{\text{mphp}}^{\text{comm}}$	$R$
15 Apr	2856	4.63	2.43	5.67	2.66	0.21
18 Apr	1008	2.30	1.81	3.52	2.16	-0.31
19 Apr	3285	1.77	0.94	1.81	1.32	-0.08
03 May	525	5.04	3.69	5.97	3.79	-0.36
07 May	3814	3.08	3.88	3.16	3.28	0.53
12 May	1188	4.86	5.26	4.25	5.26	-0.20
13 May	13 741	3.55	2.62	3.32	2.57	0.12
16 May	2995	5.45	6.13	5.53	6.06	0.19

[Title Page](#)
[Abstract](#)
[Introduction](#)
[Conclusions](#)
[References](#)
[Tables](#)
[Figures](#)
[◀](#)
[▶](#)
[◀](#)
[▶](#)
[Back](#)
[Close](#)
[Full Screen / Esc](#)
[Printer-friendly Version](#)
[Interactive Discussion](#)


## Ash plume top height estimate using AATSR

T. H. Virtanen et al.

**Table 4.** Daily average heights (standard deviations) for the Eyjafjallajökull eruption and mask fractions for day time orbits.  $N$  is the number of pixels with a valid height estimate, and bav frac. gives the fraction of filtered (best average height) pixels. The other fractions give the portion of pixels flagged by the cloud and shadow masks. In addition to the best average heights (BAV) and single pixel heights (SPH) calculated with the largest correlation window size (CWS  $11 \times 11$ ) we show the single pixel height calculated simultaneously with two smaller correlation window sizes, the medium window height (MwH,  $9 \times 9$ ), and the small window height (SwH,  $7 \times 7$ ). Heights are given in kilometers a.s.l.

Date	$N$	bav frac.	Cld frac.	Shd frac.	BAV	SPH	MwH	SwH
15 Apr	11 641	24.0%	43.3%	28.2%	5.03 (3.1)	3.84 (3.5)	4.08 (3.6)	4.52 (3.8)
16 Apr	7333	0.9%	97.4%	26.2%	1.41 (1.1)	4.17 (3.9)	4.48 (4.0)	4.93 (4.1)
17 Apr	14 529	48.0%	4.9%	12.1%	1.96 (1.0)	1.59 (1.6)	1.84 (2.1)	2.47 (2.9)
04 May	4431	10.5%	65.1%	12.6%	1.14 (0.3)	2.58 (3.2)	2.87 (3.6)	3.44 (3.9)
06 May	57 360	26.0%	64.4%	11.7%	3.09 (1.5)	4.70 (2.3)	4.72 (2.4)	4.86 (2.7)
07 May	132 809	8.2%	83.1%	30.8%	2.81 (1.9)	4.36 (3.4)	4.57 (3.5)	4.87 (3.7)
08 May	86 780	25.7%	46.9%	35.1%	2.03 (1.9)	3.28 (3.3)	3.64 (3.6)	4.17 (3.9)
09 May	103 825	25.6%	19.0%	23.7%	2.64 (2.4)	2.13 (3.0)	2.50 (3.3)	3.11 (3.6)
10 May	26 400	19.7%	47.0%	21.1%	2.58 (2.0)	2.24 (2.9)	2.65 (3.2)	3.26 (3.5)
11 May	5418	40.8%	27.6%	18.7%	3.78 (1.7)	3.14 (2.1)	3.41 (2.4)	3.80 (2.9)
12 May	8801	20.4%	69.2%	16.6%	4.53 (1.6)	4.28 (1.9)	4.37 (2.1)	4.56 (2.4)
13 May	69 639	39.3%	37.7%	23.8%	3.97 (1.4)	4.23 (2.2)	4.42 (2.5)	4.77 (2.9)
14 May	51 443	32.2%	42.7%	24.0%	3.96 (2.2)	3.85 (2.7)	4.06 (2.9)	4.44 (3.2)
15 May	65 697	33.0%	28.5%	21.5%	2.81 (1.9)	2.37 (2.5)	2.69 (2.8)	3.23 (3.2)
16 May	44 271	15.5%	45.7%	26.4%	4.13 (2.1)	3.09 (3.1)	3.38 (3.2)	3.88 (3.4)
17 May	89 623	9.8%	66.8%	34.6%	3.72 (2.8)	2.99 (3.6)	3.48 (3.8)	4.13 (4.0)
18 May	26 877	22.5%	60.4%	26.1%	6.03 (2.6)	4.59 (3.3)	4.76 (3.5)	5.01 (3.6)
Total	806 877	22.5%	54.3%	26.9%	3.21 (2.2)	3.41 (3.2)	3.70 (3.3)	4.15 (3.6)

Title Page

Abstract Introduction

Conclusions References

Tables Figures

◀ ▶

◀ ▶

Back Close

Full Screen / Esc

Printer-friendly Version

Interactive Discussion



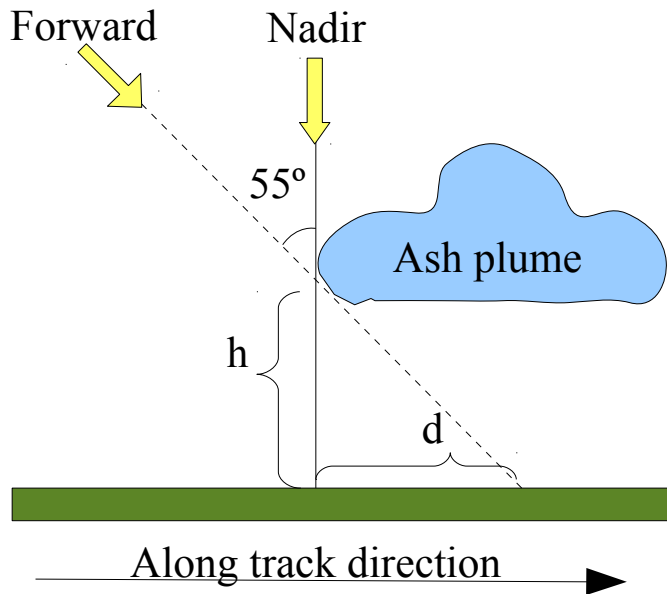


**Fig. 1.** Cloud height estimate geometry. The edge of the cloud (at altitude  $h$ ) is observed at different apparent positions at the ground level in the two views, with distance  $d$ . With increasing height the distance increases.

**Ash plume top height estimate using AATSR**

T. H. Virtanen et al.

Title Page	
Abstract	Introduction
Conclusions	References
Tables	Figures
◀	▶
◀	▶
Back	Close
Full Screen / Esc	
Printer-friendly Version	
Interactive Discussion	



## Ash plume top height estimate using AATSR

T. H. Virtanen et al.

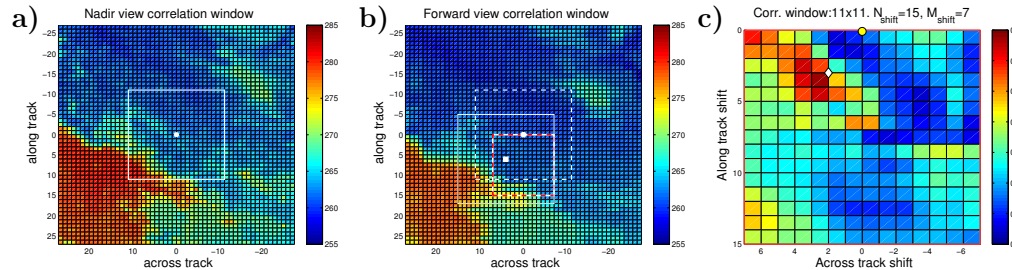


**Fig. 2.** Illustration of the cross correlation coefficient method using  $10.85\ \mu\text{m}$  channel data ( $T_{11}$ ). The nadir view reference window is held in place **(a)**, while the center point of the forward view target window is allowed to move within the pre-set shift window shown as the red-and-white rectangle **(b)**. The forward view window scans all allowed shifts, and the resulting cross correlation matrix is shown at panel **(c)**. The maximum value of cross correlation coefficient  $C$  determines the best-fitting shift  $(m, n)$  selected by the algorithm. In this example, the algorithm picks shift  $(2, 3)$  as the maximum correlation shift.

## Ash plume top height estimate using AATSR

T. H. Virtanen et al.

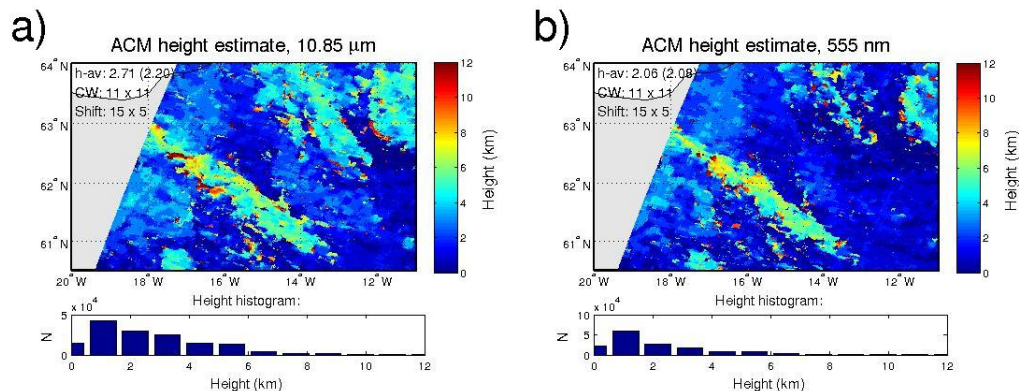


**Fig. 3.** Effect of wavelength on a full scene height retrieval. The height maps show the ACM single pixel height estimates (km a.s.l.) for an Eyjafjallajökull ash plume and its surroundings on 16 May 2010, obtained at two wavelengths, 10.85  $\mu\text{m}$  and 555 nm, respectively. The height histograms below the maps show number of pixels within each height bin. See text for details.

## Ash plume top height estimate using AATSR

T. H. Virtanen et al.

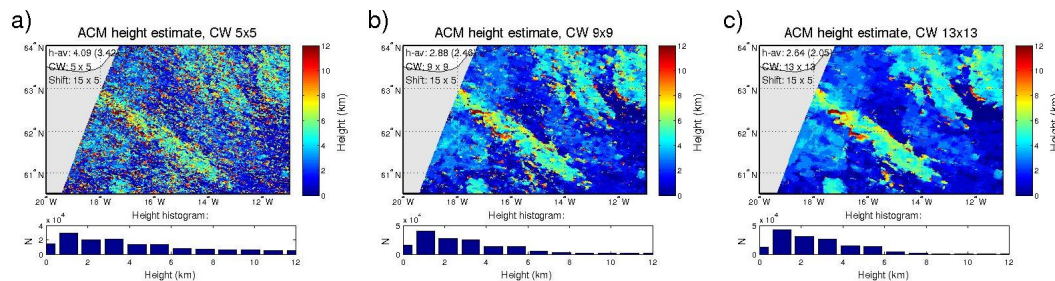


**Fig. 4.** AATSR height estimate with three different CW sizes,  $5 \times 5$ ,  $9 \times 9$ , and  $13 \times 13$ . The average height for the full scene varies in the range 2.6–4.1 km for all CWS, but settles at  $\sim 2.6$  km when CWS is increased. Also, the standard deviation of height decreases with increasing CWS. The height histograms below the height maps show how the fraction of high-altitude pixels decreases with increasing CWS.

[Title Page](#)
[Abstract](#)
[Introduction](#)
[Conclusions](#)
[References](#)
[Tables](#)
[Figures](#)
[◀](#)
[▶](#)
[◀](#)
[▶](#)
[Back](#)
[Close](#)
[Full Screen / Esc](#)
[Printer-friendly Version](#)
[Interactive Discussion](#)


## Ash plume top height estimate using AATSR

T. H. Virtanen et al.

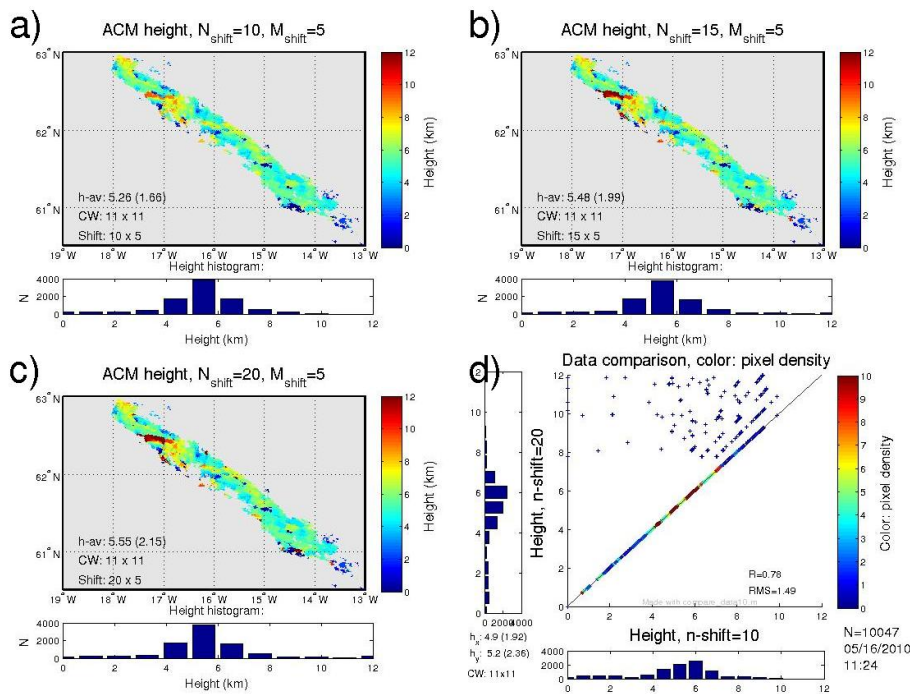


**Fig. 5.** Effect of the maximum allowed along-track shift,  $N_{\text{shift}}$  (or  $N$ ). Color scale is limited to 0...9 km although larger heights are possible, as seen in the height histograms (at the bottom of the figures). We see that most of the changes appear for the highest parts of the plume (as expected), but the scatter plot indicates other differences as well.

Title Page

Abstract

Introduction

Conclusions

References

Tables

Figures

◀

▶

◀

▶

Back

Close

Full Screen / Esc

Printer-friendly Version

Interactive Discussion



## Ash plume top height estimate using AATSR

T. H. Virtanen et al.

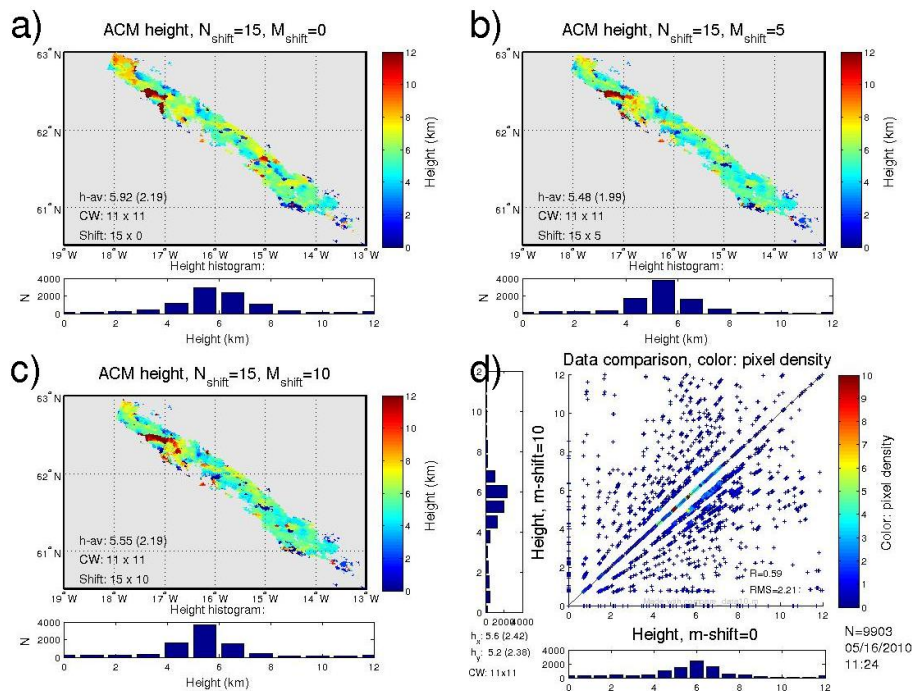


**Fig. 6.** Effect of the maximum allowed across-track shift,  $M_{\text{shift}}$  (or  $M$ ), is much larger than that of  $N_{\text{shift}}$ . However, the difference between  $M = 5$  and  $M = 10$ , for example, is already much smaller ( $R = 0.89$ , not shown) than between  $M = 0$  and  $M = 10$  shown here ( $R = 0.59$ ).

Title Page

Abstract

Introduction

Conclusions

References

Tables

Figures

◀

▶

◀

▶

Back

Close

Full Screen / Esc

Printer-friendly Version

Interactive Discussion



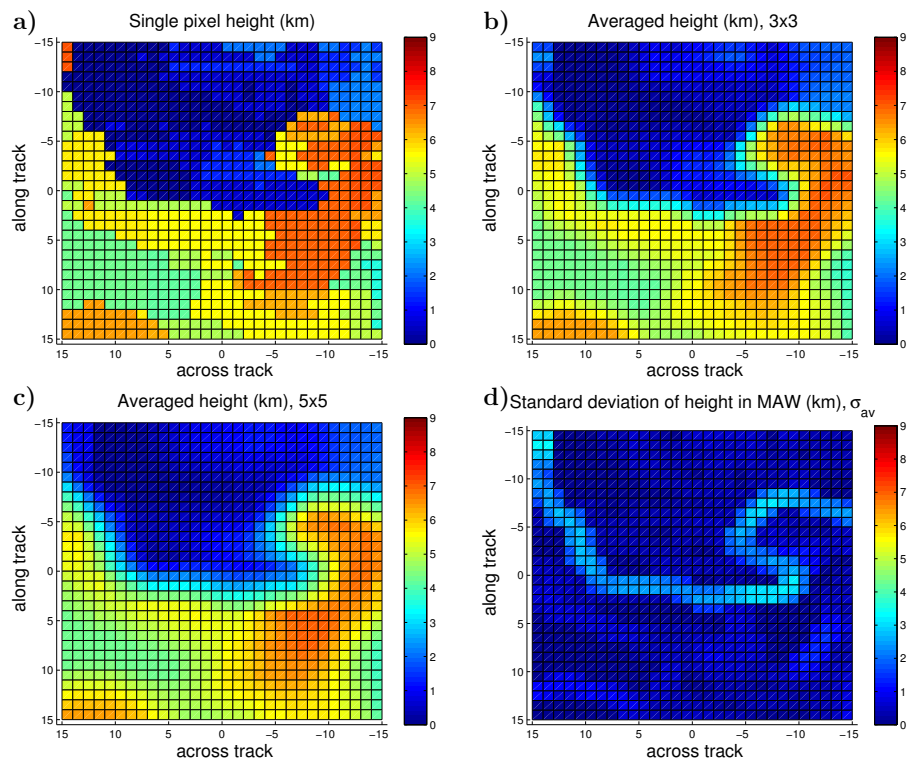


**Fig. 7.** The effect of the averaging with a moving averaging window (MAW). **(a)** The initial single pixel heights; **(b)** the MAW size  $3 \times 3$  averaged values; **(c)** the MAW size  $5 \times 5$  values. The averaging smooths the data, removing isolated peaks, but some details are lost. **(d)** The standard deviation of height within the MAW clearly indicates the plume edges.

Ash plume top height estimate using AATSR

T. H. Virtanen et al.

Title Page

Abstract

Introduction

Conclusions

References

Tables

Figures

◀

▶

◀

▶

Back

Close

Full Screen / Esc

Printer-friendly Version

Interactive Discussion



## Ash plume top height estimate using AATSR

T. H. Virtanen et al.

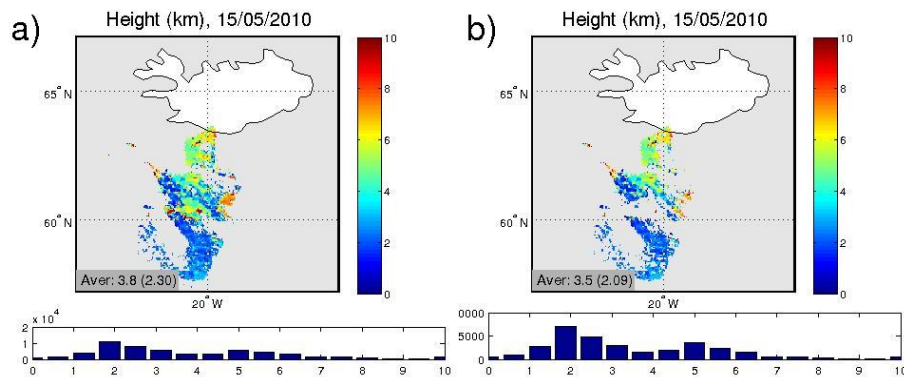


**Fig. 8.** Eyjafjallajökull eruption 15 May 2010. We show the effect of removing the ash pixels flagged as cloudy by 659 nm reflectance cloud test. In panel (a) we show all SPH values, while in panel (b) the cloud flagged pixels have been removed. The average height decreases from 2.40 km to 2.29 km when the clouds are removed, but the height histograms (below the maps) show that there are no dramatic changes in the height distribution.

Title Page

Abstract

Introduction

Conclusions

References

Tables

Figures

◀

▶

◀

▶

Back

Close

Full Screen / Esc

Printer-friendly Version

Interactive Discussion



## Ash plume top height estimate using AATSR

T. H. Virtanen et al.

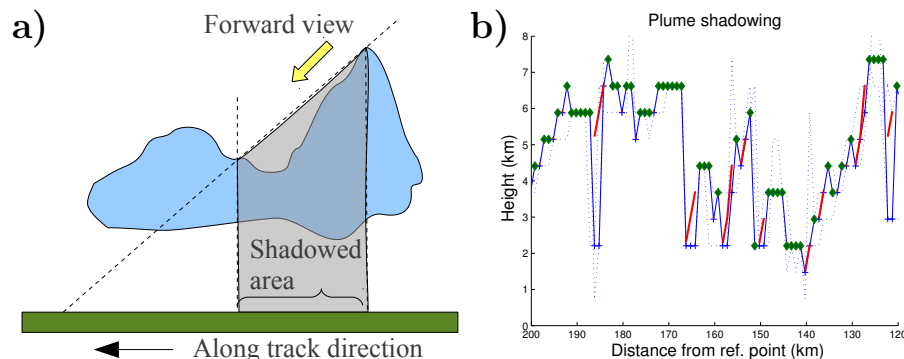


**Fig. 9.** (a) Principle of the plume shadowing. A high feature can block the forward view (for lower features) in the along-track direction. A reliable height estimate cannot be obtained for pixels in the shadowed area. (b) An example of shadow masking, an along-track height profile. The blue line shows the initial height estimate. The high features block the forward view on the areas indicated by the red lines, preventing the height estimate. The green dots indicate heights accepted after the shadow masking. Note that in the shadowed areas the method typically suggests uniform, underestimating heights.

## Ash plume top height estimate using AATSR

T. H. Virtanen et al.

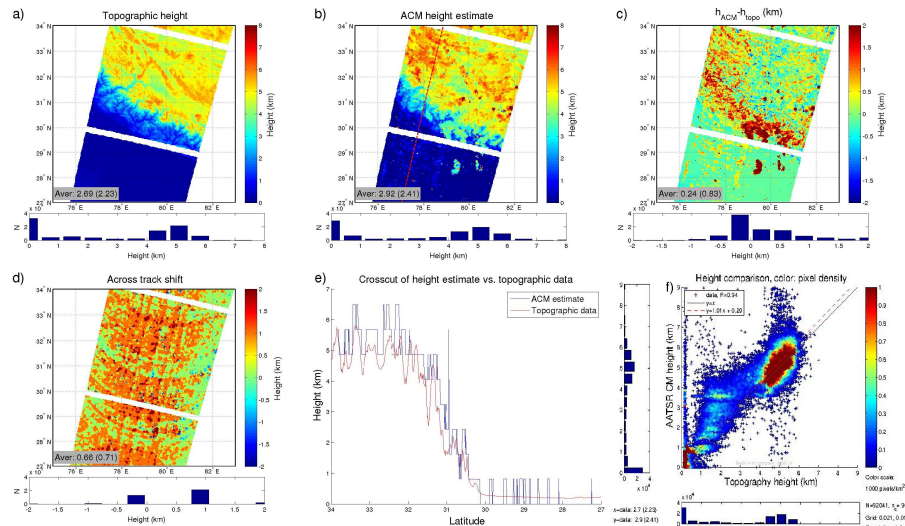


**Fig. 10.** (a) Topographic data over Himalayas, (b) AATSR height estimate, (c) their difference, (d) the across-track pixel shift, (e) a crosscut height profile, and (f) the scatter plot for topographic height and ACM estimate. Some cloud contamination can be seen in the ACM height estimate, particularly on the southern edge of the mountain range. These cause the largest differences, seen as the red areas in panel (c), narrow peaks in panel (f) and as large scatter in panel (d). The crosscut is indicated in panel (b) as the dashed red line. The vertical resolution of roughly 1 km is clearly seen in the height estimate profile (f), as well as the jumping of the algorithm between 0 and 1 km in the lower plains. Panel (d) shows features resembling the conical scanning geometry of AATSR, and may indicate ground level collocation errors.

## Ash plume top height estimate using AATSR

T. H. Virtanen et al.

Title Page

Abstract

Introduction

Conclusions

References

Tables

Figures



Back

Close

Full Screen / Esc

Printer-friendly Version

Interactive Discussion

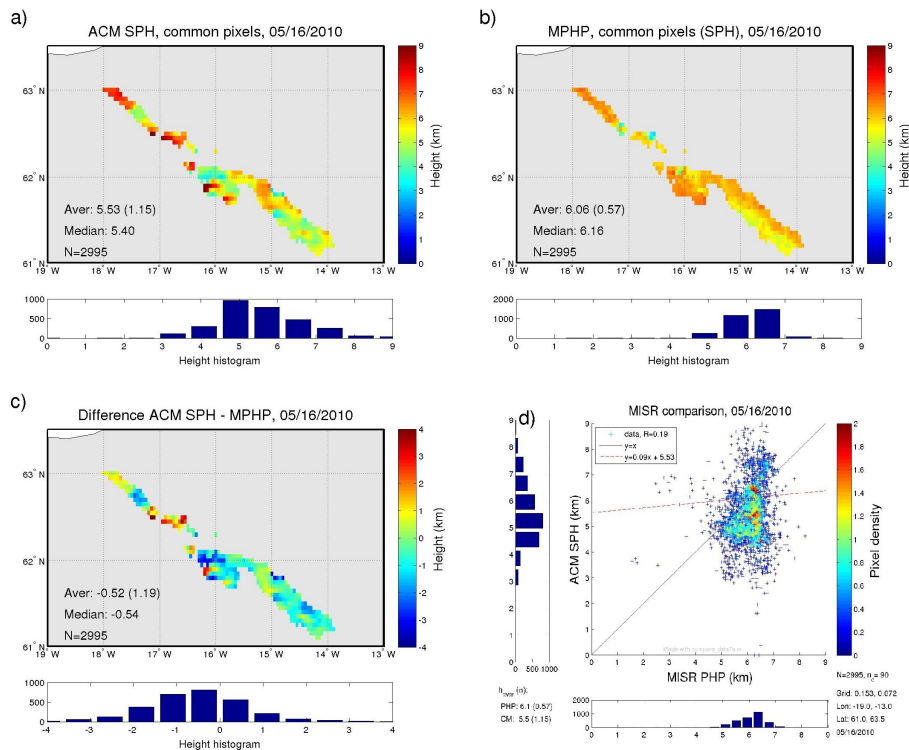


**Fig. 11.** The MPHP and ACM (SPH) plume heights and their difference, limited by both the MPHP plume and AATSR-detected ash plume ( $BTD < 0$  K). AATSR gives 0.5 km lower heights on average, with significantly more variation ( $\sigma_h = 0.6$  km for MISR and  $\sigma_h = 1.2$  km for AASTR), as can be seen from the height histograms (below the height maps). The differences are centered roughly at zero, but the scatter plot shows poor pixel-by-pixel correlation ( $R = 0.2$ ) between the instruments.

## Ash plume top height estimate using AATSR

T. H. Virtanen et al.

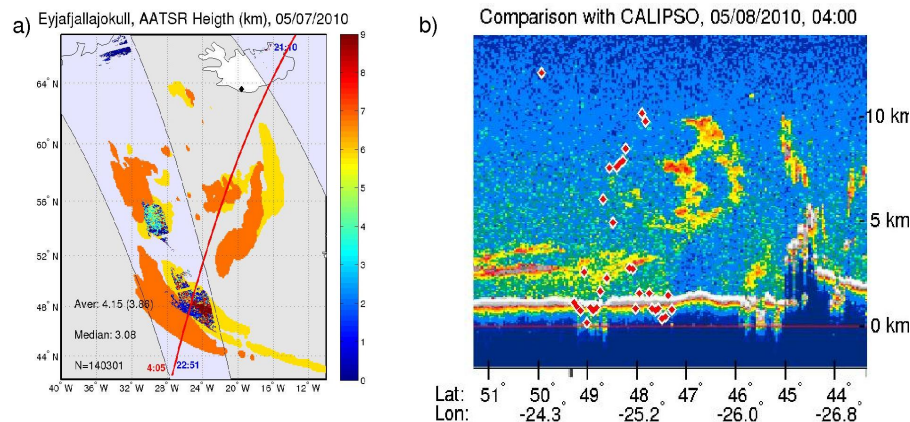


**Fig. 12.** Eyjafjallajökull eruption, 7–8 May 2010; a near simultaneous overpass of AATSR and CALIPSO over a large ash cloud. **(a)** The shaded blue area shows the AATSR swath on 7 May at approximately 22:51, while the red line shows CALIPSO track on 8 May at approximately 4:05. The color-coded pixels show the ACM height estimate. The yellow area shows ash plume detected by SEVIRI on 7 May at 23:00, which coincides with the ACM plume (within the AATSR swath). The orange area shows the plume observed by SEVIRI five hours later, at the time of CALIPSO overpass. **(b)** CALIOP backscatter profile on 8 May at 04:00, with the ACM height estimates from 7 May 22:51 shown by the red symbols. The ash plume is seen between 46–48° N in the back scatter data, while for ACM it was observed near 48–49° N.

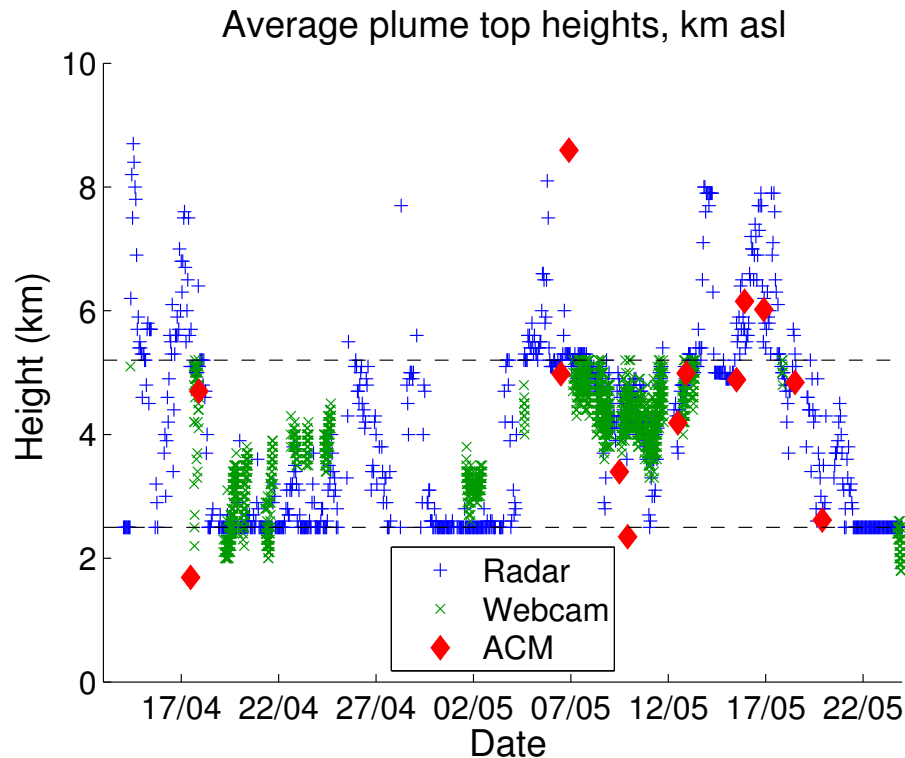


**Fig. 13.** Ground based plume top height data for Eyjafjallajökull plume from the Keflavík weather radar and a web camera at Hvolsvöllur (Arason et al., 2011), combined with the AATSR height estimates near the volcano. The radar data is limited from below by 2.5 km and the web camera data is limited from above to 5.2 km (dashed black lines). The ACM data is an average over all ash-flagged single pixel heights within 50 km from the volcano (both day and night time data).

**Ash plume top height estimate using AATSR**

T. H. Virtanen et al.

Title Page	
Abstract	Introduction
Conclusions	References
Tables	Figures
◀	▶
◀	▶
Back	Close
Full Screen / Esc	
Printer-friendly Version	
Interactive Discussion	



## Ash plume top height estimate using AATSR

T. H. Virtanen et al.

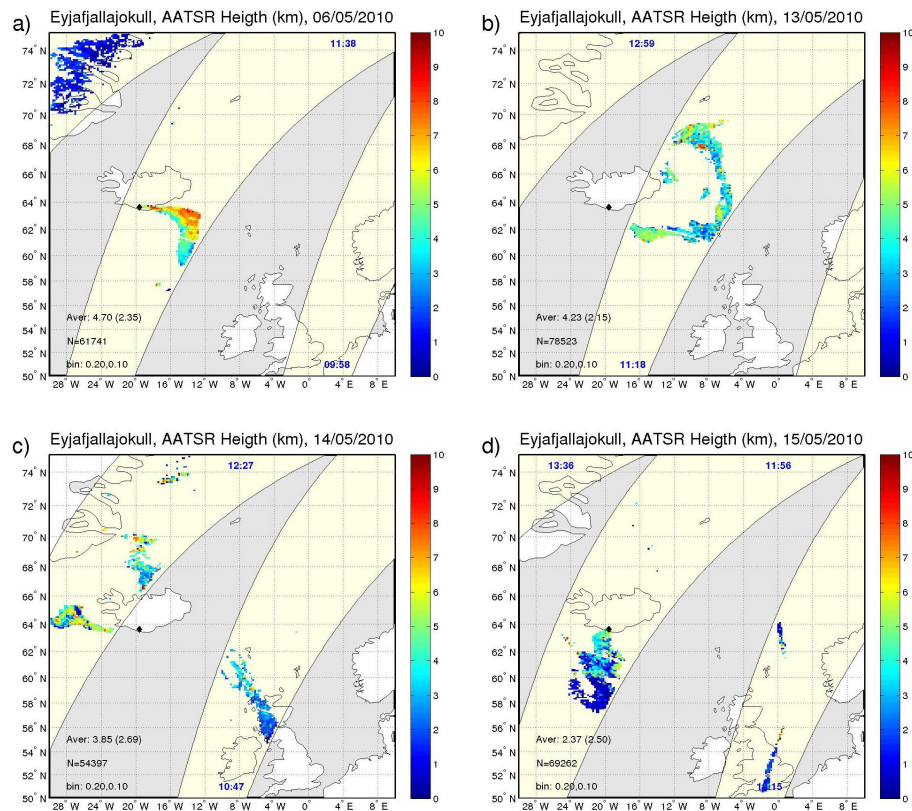


**Fig. 14.** Single pixel height for selected plumes on four days in May 2010. The yellow shaded areas show the AATSR swath, with the blue numbers giving the UTC time of the orbit. The color-coded pixels give the ACM height estimate (km a.s.l.). The text inserts in the lower left show the average height (standard deviation) and the number of pixels  $N$  in each image.

## Ash plume top height estimate using AATSR

T. H. Virtanen et al.

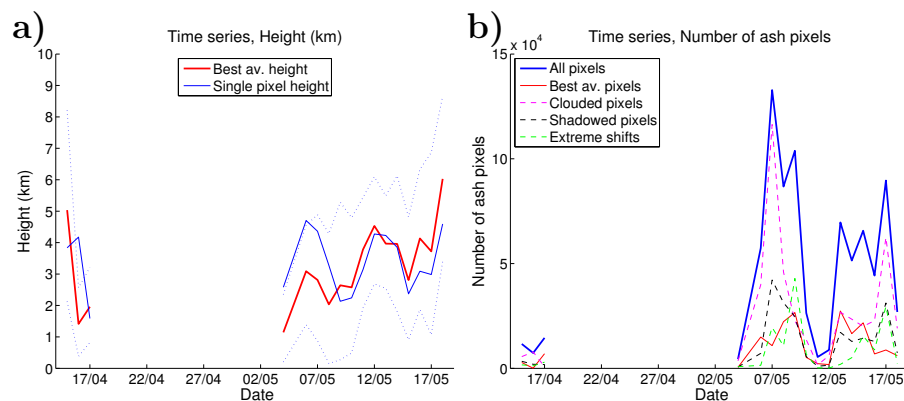


**Fig. 15.** Time series of daily average heights and number of ash pixels. The blue lines give the average values using all pixels (SPH), and the red lines give average values using the filtered pixels only (BAV). The dotted blue lines on the left show the error bars (standard deviation). On the right we show also the number of pixels flagged as clouded or shadowed, and also the number of pixels with an extreme (maximum or zero) along-track pixel shift.

[Title Page](#)
[Abstract](#)
[Introduction](#)
[Conclusions](#)
[References](#)
[Tables](#)
[Figures](#)
[Back](#)
[Close](#)
[Full Screen / Esc](#)
[Printer-friendly Version](#)
[Interactive Discussion](#)

## Ash plume top height estimate using AATSR

T. H. Virtanen et al.

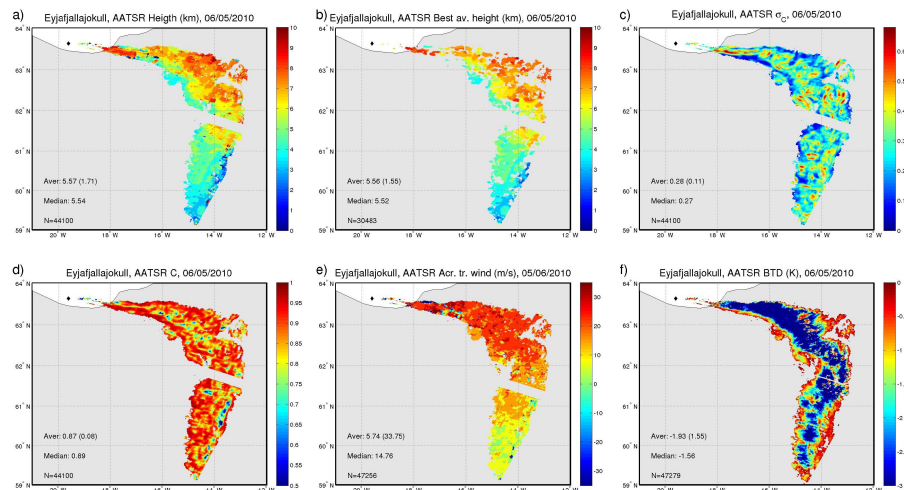


**Fig. 16.** Example case of 6 May 2010 over Iceland. **(a)** Single pixel height estimate; **(b)** best average height estimate; **(c)** standard deviation of  $C$  within the correlation matrix; **(d)** the cross correlation coefficient  $C$ ; **(e)** the across-track wind speed ( $\text{m s}^{-1}$ ); **(f)** the brightness temperature difference BTM (scale limited to  $-3\text{K}$ ). The text inserts on the lower left hand corners of the images show the average value (standard deviation) and median of each quantity, and the number of pixels used. See text for details.

Title Page

Abstract

Introduction

Conclusions

References

Tables

Figures

◀

▶

◀

▶

Back

Close

Full Screen / Esc

Printer-friendly Version

Interactive Discussion

